U.S. Department
of Transportation

Volpe National
Transportation Systems
Center

55 Broadway
Cambridge, MA 02142

Memorandum

Subject:	Polar Source Analysis	Date:	9/29/2017
From:	Eric Boeker (Volpe), Juliet Page (Volpe), Chris Cutler (Volpe)	Reply to Attn. of:	V0324
To:	Hua He (FAA AEE)	FAA Report No.:	DOT/FAA/AEE/2018-02
CC:	Becky Cointin (FAA AEE), Chris Roof (Volpe)	Volpe Report No.:	DOT-VNTSC-FAA-18-02

The following technical memorandum describes the development, testing and analysis of various polar source data sets. The memorandum also includes recommendation for potential inclusion in future releases of AEDT. This memorandum is the final deliverable of FA5JCK00 PA423 “Ray Tracing Model Development”, which was re-scoped from ray model development to polar source analysis in 2016.

1 Introduction

FAA AEE’s Aviation Environmental Design Tool (AEDT) and other aircraft, environmental, acoustic research tools are used to evaluate the effects of noise generated by aircraft at known receptors in the vicinity of airports, flight paths, air tour routes and other aircraft operations[1]. In recent years, numerous research efforts, including FAA’s Center of Excellence for Alternative Jet Fuels and Environment (ASCENT) and Transportation Research Board Airport Cooperative Research Program (TRB ACRP) projects, have focused on expanding and improving the noise modeling methods used in these FAA AEE tools. However, these improved noise modeling methods are limited by the fidelity of the source noise data.

The purpose of this project was to evaluate options for developing more detailed acoustic source models of aircraft, and to provide recommendations on developing those data and leveraging them to improve computational capabilities in FAA AEE’s environmental tools, including both the Aviation Environmental Design Tool (AEDT) and other FAA AEE research tools.

This effort specifically focused on reviewing three-dimensional (3-D) polar source development options and recommending a process for moving forward that is implementation ready and has undergone preliminary validation.

Vehicle noise emission condition is generally a function of operating state and configuration, and may be described using lateral and longitudinal directivity and spectral information. The most generalized form is a three-dimensional polar spectral noise source. Any arbitrary compact source or collection of compact sources may be defined by polar spectral source, with varying spectral and level emission in all directions as a function of vehicle condition (speed, operating and maneuvering state, orientation, configuration etc.) While the NPD database is predicated on an infinite segment length of a constant condition moving source and integrated metric value for the entire operation assuming a reference propagation and atmosphere, this restriction is removed in polar sources, also permitting easy modeling of stationary sources.

For this effort, polar noise sources were initially built from legacy data and AEDT 2b directivity procedures. This analysis shows that the various directivity techniques are relatively consistent with existing AEDT results for under-track centerline analyses. Moving to this structure allows the possibility for higher fidelity improvements leveraging existing, future measurements and analytical capabilities, such as those being explored in ASCENT projects addressing approach configuration modeling (i.e., ASCENT Project 43 "Noise Power Distance Re-Evaluation")[2]. The polar database could be structured with the ability to consider new vehicle types such as Blended Wing Body aircraft (BWBs), Unmanned Aerial Vehicles (UAVs) and tiltrotors and other operational modes such as different vehicle configurations (gear/flaps) and operating state (speed, flight path angle) based sources and new modes such as taxi and reverse thrust.

This project was comprised of three separate tasks:

1. Review 3-D polar source generation methods;
2. Develop 3-D polar sources from existing data with existing tools and evaluate results; and
3. Document the 3-D polar source development recommendations.

For the first task, existing methods and tools for generating polar acoustic sources for aircraft were reviewed and evaluated (see Section 2). The second task focused on a recommended method for developing 3-D polar source data by conducting a feasibility study that resulted in the development of 3-D polar sources for several example fixed wing aircraft, utilizing and fine-tuning the recommended methods from the first task (see Sections 3 and 4). In addition, AEDT implementation considerations are also presented (see Section 5). The third task is satisfied by this technical memorandum.

2 Polar Source Data Review

The polar source data review consisted of three sub-tasks: a review of the data currently in AEDT, a review of methods currently available for polar source development, and a review of data available to be used in those methods to generate polar sources.

2.1 Data Currently in AEDT

The source noise data in AEDT consist of noise-power-distance data, spectral classes and directivity.

Noise-power-distance data (NPDs) represent the integrated aircraft source noise level for an infinite constant condition segment, given operational mode and power setting at a range of slant distances from the aircraft which account for acoustic propagation through a standard atmosphere[1]. NPDs represent the source noise for a specific aircraft performing a specific type of operation. NPDs also include the complete noise generated by all components (airframe and all engines including any interaction effects such as engine integration and shielding, and main/tail rotor, wake and airframe interaction and engine noise for helicopters).

The AEDT database includes two types of NPDs: fixed-wing aircraft NPDs (for all commercial and military fixed wing aircraft), and helicopter NPDs. The NPD data for fixed-wing aircraft consist of a set of decibel (dB) levels for various combinations of aircraft operational modes, engine power settings, slant distances from aircraft to receptor, and base noise metrics that are associated with a specific aircraft model*. The NPD data for helicopters consist of a set of decibel levels for various combinations of aircraft operational modes, slant distances from aircraft to receptor, and base noise metrics that are associated with a specific helicopter engine. Helicopter NPDs are also represented by a set of three NPDs for each operational mode, in order to better represent helicopter noise directivity for moving (or dynamic) operations. The three curves correspond to noise levels at locations directly below the helicopter (center) and at approximately 45 degrees to either side (left/right) of the centerline.

The spectral class data in AEDT consist of a set of sound pressure level vs. one-third octave-band frequency (50 Hz to 10 kHz) values corrected to a reference distance of 1,000 ft (305 m) using the SAE-AIR-1845[2] atmospheric absorption coefficients. Since AEDT does not support a separate spectrum for each aircraft and operational mode, the AEDT database is populated with spectral classes, which represent the spectral shape at time of maximum sound level for a group of aircraft deemed to have similar spectral characteristics for each different operation mode (approach, departure, level flight/afterburner). Each fixed-wing aircraft has a single spectral class of departure operations and another for approaches. In addition, helicopters have a level flight spectral class, and military aircraft have an afterburner spectral class.

Directivity data in AEDT comes from a number of sources. For all aircraft in AEDT, directivity is represented by two adjustments: noise fraction and lateral attenuation[1]. The noise fraction adjustment is the fractional noise exposure associated with a finite-length flight path segment, based upon a fourth-power, 90-degree dipole model of sound radiation. The lateral attenuation adjustment accounts for the difference in level between the sound directly under the aircraft's flight path and at a location to the side of the aircraft at the time of closest approach, and it combines effects on aircraft sound due to 1) over-ground propagation: ground reflection effects, refraction effects, and 2) effects due to aircraft source noise emission: airplane shielding and engine installation effects. The lateral attenuation adjustment in AEDT is based on SAE-AIR-5662[4].

In addition to Noise Fraction and Lateral Attenuation, a behind-start-of-takeoff-roll directivity adjustment is applied to ground roll segments for fixed-wing aircraft. The behind-start-of-takeoff-roll directivity in AEDT is currently based on SAE-AIR-1845[2], and it is scheduled to be updated to a method based on SAE-AIR-6297 in the near future[5]. For helicopters, directivity is represented by the helicopter NPDs for dynamic operations, and by a directivity data set for hover and idle (or static) operations. This static directivity data account for changes to the sound level as a function of the helicopter azimuth angle.

* A specific model may include a particular engine or hush kit or other modifications.

In summary, fixed-wing aircraft noise sources are represented in AEDT by single operation-specific, thrust-specific noise levels (NPDs) and a single operation-specific spectrum (spectral classes), which are modified by several directivity adjustments (noise fraction, lateral attenuation, and behind start-of-takeoff-roll directivity). Helicopter noise sources are represented in AEDT by a set of three operation-mode-specific noise levels (NPDs) and a single operation-specific spectrum (spectral classes), which are modified by several directivity adjustments (noise fraction, lateral attenuation, and static directivity). While some aircraft noise directivity is represented in the current AEDT database, it does not fully represent the range of noise level, spectra and directivity changes that occur over a range of aircraft operations. For example, on takeoff (including for reduced thrust takeoffs or during cutback) the noise emission is predominately driven by engine noise due to the higher thrust setting. However during approach, especially for newer model aircraft, the engines are not producing much thrust and the complex airframe noise with different directivity and spectral content dominates the noise emission. A significant amount of NASA sponsored research including wind tunnel and flight testing has developed improved noise source modeling for landing gear, flaps, slats, shielding and other forms of airframe noise[5,6,7,8,9,10,11,12,13]. Updating AEDT to incorporate polar source formulation will allow a more rapid incorporation of these airframe noise effects in the future. ASCENT project 43 looking at NPDC (where the C refers to configuration) includes an update to the NPD however it only addresses the centerline noise change reflected in the NPD and spectral class and does not include any lateral or fore/aft directivity improvements[2]. Transition to a polar source is required to capture those effects.

2.2 Existing Methods for Polar Source Development

For this task, existing methods and tools for generating polar acoustic sources for aircraft were reviewed and evaluated. This review included the following tools and methods: DOD source development process, NASA's AAM, and the aircraft noise modeling tools developed by EMPA (the Swiss Federal Laboratories for Materials Science and Technology). This review also included related work that also explores more complex acoustic sources for aircraft, advanced acoustic propagation modeling, and the interactions between the two, including NASA's ANOPP, and relevant FAA ASCENT research, among others.

2.2.1 Leveraging AEDT for Polar Source Development

Both the FAA's AEDT model and the DOD NOISEMAP rely on integrated metric source noise databases. AEDT source data is embodied in NPDs, while the DOD NOISEFILE data, maintained by the Air Force Research Laboratory (AFRL), contains spectral data at a single reference distance (1000 ft.) which is then pre-propagated to other distances using the OMEGA preprocessor. OMEGA utilizes the user defined atmosphere conditions (temperature and humidity) to obtain pre-propagated integrated levels at other distances. The combination of NOISEFILE + OMEGA is functionally equivalent information to the NPDs in AEDT. The standardization of 1000 ft and corrections to other distances is noted and was leveraged in the development of polar sources for this project.

Within AEDT there is some limited directivity data for fixed wing aircraft. Lateral directivity is prescribed based on whether the engines are wing or fuselage mounted and is graphically represented in Figure 1 as described in SAE-AIR-5662[4]. This lateral directivity data was used to develop polar noise sources for this project.

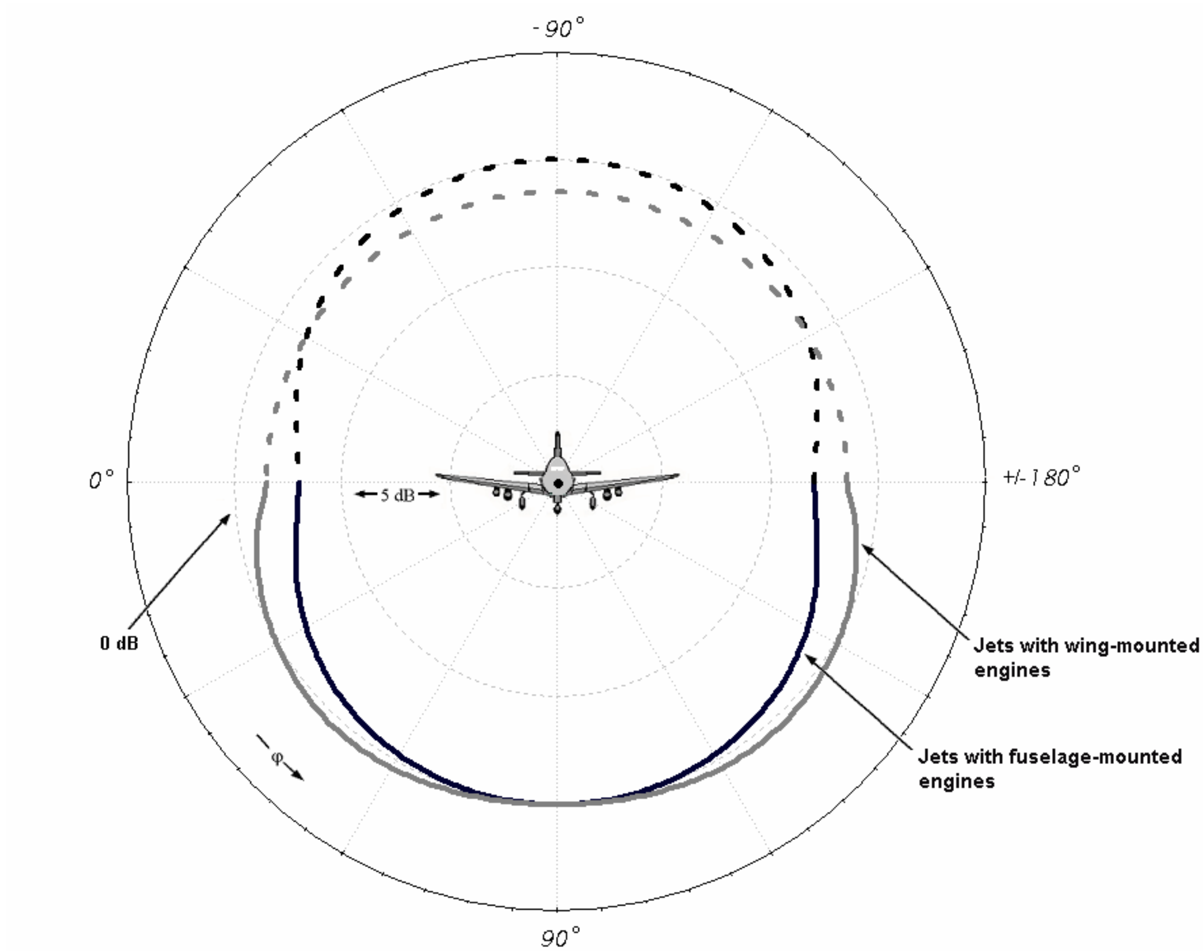

Figure 1. Lateral Directivity Engine Installation Source adjustment in AEDT

During the start-of-takeoff-roll, AEDT applies a directivity correction to the propagation results. This single directivity is applied to all jet aircraft and was determined empirically and adjusted based on the US Fleet mix. The directivity is defined as a function of polar angle relative to the aircraft orientation. This directivity shape behind the aircraft could be used to develop polar noise sources. AEDT employs basic assumptions which simplify computational requirements. These assumptions include time-integrated noise exposure, flat earth, uniform atmospheric conditions, linear acoustic propagation, no wind effects, and minimal aircraft directivity. Two versions of the AEDT behind start-of-takeoff-roll directivity were used for this analysis: the directivity currently used in AEDT based on SAE-AIR-1845[3], and the updated based on SAE-AIR-6297[5] which is planned for use in future versions of AEDT (see Figure 2).

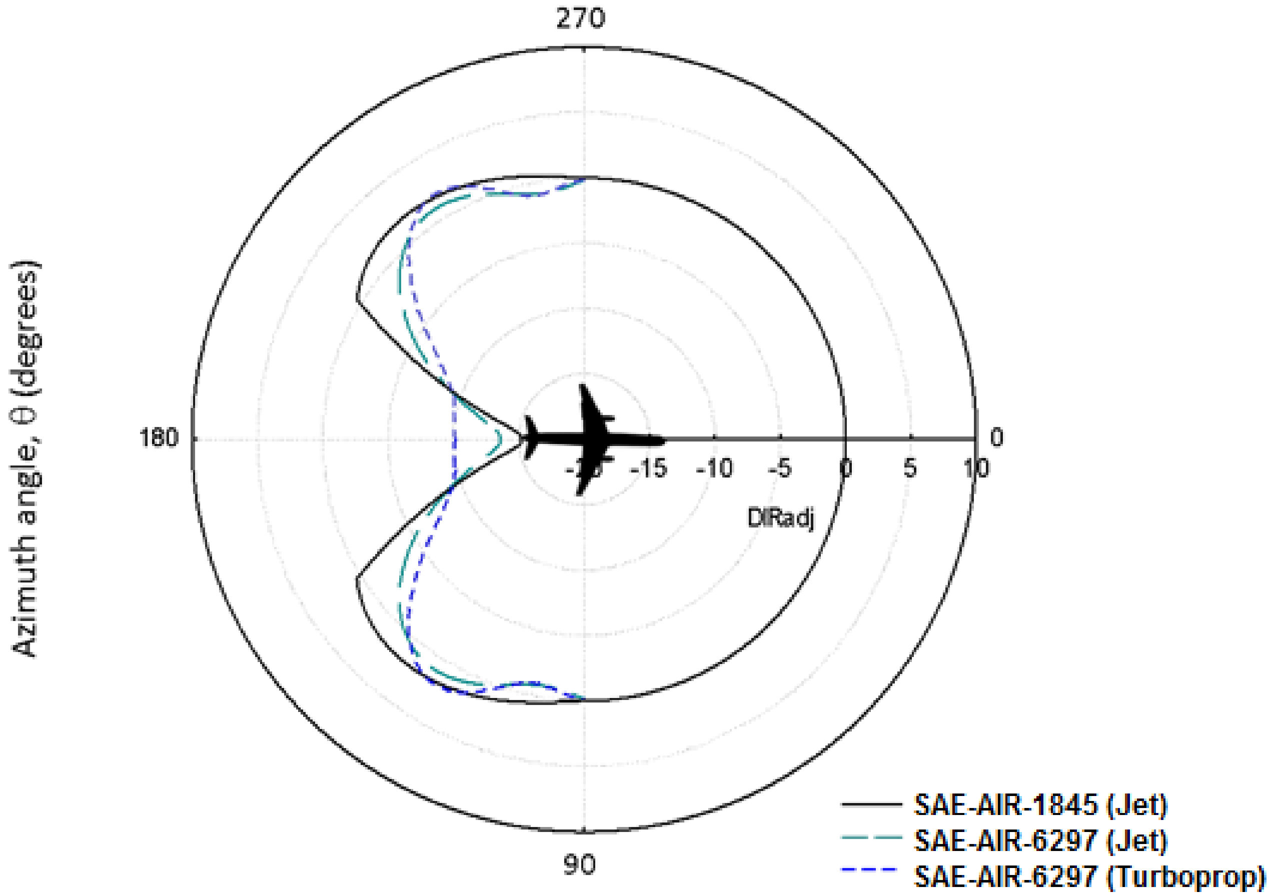

Figure 2. SAE-AIR-1845 (in AEDT 2) and SAE-AIR-6297 (Scoped for AEDT 3) Start-of-Takeoff-Roll Directivities[4]

An example of an omnidirectional polar source adjusted to include SOTR directivity and lateral attenuation is presented in Figure 3.

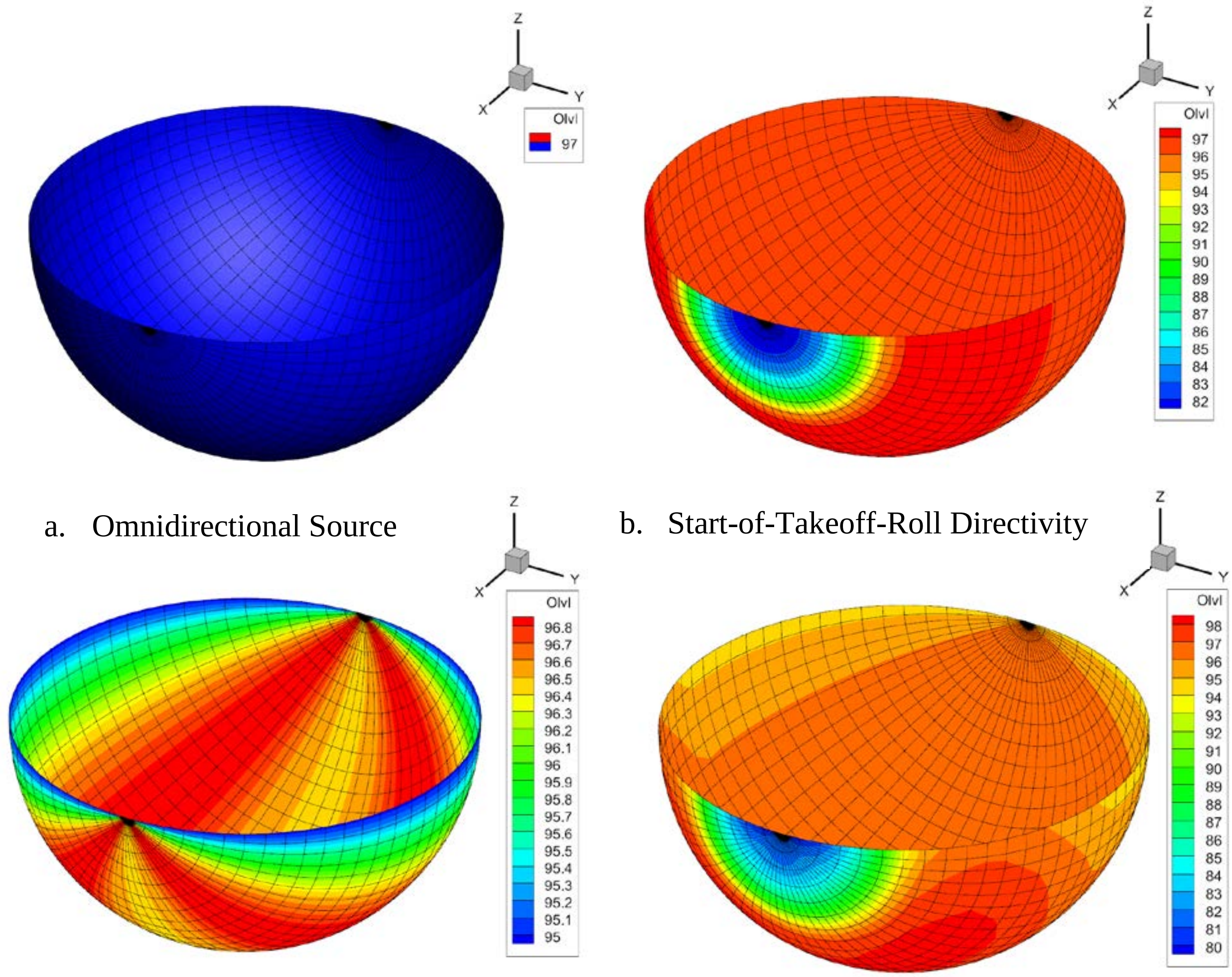

a. Omnidirectional Source

b. Start-of-Takeoff-Roll Directivity

c. Lateral Attenuation

d. Final Source including a, b and c

Figure 3. Example of Combining Directivity Data to Form a Polar Source: a. Omnidirectional Source, b. Start-of-Takeoff-Roll Directivity, c. Lateral Attenuation and d. the Final Source

2.2.2 Techniques to Create Polar Noise Sources from Legacy Integrated Model Data

Populating an aircraft noise sphere database can be a significant obstacle to widespread adoption of simulation noise modeling to predict environmental noise impact. Simulation noise modeling has already been adopted by the DOD for the next generation of fighter aircraft, and significant work has been completed to develop methods for synthesizing noise spheres from legacy data[15,16]. The DOD is also committed to transition to the Advanced Acoustic Model and is funding development of polar noise source data for the full inventory of aircraft in the NOISEFILE database. The NoiseMap Gap assessment project has also explored and identified modeling differences between NoiseMap and AEDT[29]. These techniques have also been applied to AEDT NPD data for specialized simulation modeling purposes such as with the Noise Model Simulation (NMSIM) [17,18].

Polar Source Analysis

Acoustic data may be extracted directly from AEDT databases and mapped to a polar source and combined with higher fidelity polar source data as it becomes available. The spectral directivity characteristics of a similar aircraft may be used as a surrogate, or, if such data does not exist, an omnidirectional or predefined directivity pattern will yield a source definition of no less fidelity than the integrated model database, and will allow improved modeling that accounts for such acoustic spectral and directivity effects as are created by landing gear and flaps/slats.

A multitude of techniques to increase the directional and spectral fidelity of aircraft flight noise spheres that have been synthesized from legacy data include treatment of longitudinal and lateral directivity with surrogate directivity patterns, supplemental first principles modeling, or scaled experimental or static test data. Also procedures for synthesis of aircraft static noise conditions (run-up and start of takeoff roll) have also been developed by the DOD[15]. The benefit of this research is directly applicable to polar noise source techniques explored in this task.

2.2.3 Advanced Models that Yield Polar Noise Sources and Supplemental Data for Polar Source Development

2.2.3.1 ANOPP

ANOPP2 is a physics based source modeling tool developed by NASA[19]. The Aircraft Noise Prediction Program (ANOPP) recently underwent a major revision by NASA, creating a modular API which facilitates the user community's rapid creation of new and novel configurations and the capability to model existing aircraft noise sources from first principles. The modules have been extensively validated via wind tunnel and flight acoustic testing and new capabilities in the area of distributed propulsion, airframe noise including slats, flaps and landing gear, UAVs and electric propulsion and engine technologies (acoustic liners, open rotors, core noise) are being researched at NASA[20]. With a polar source characterization, ANOPP spectral polar source output could be used by AEDT, enabling the evaluation of new configurations, procedures and technologies environmental impacts.

The Environmental Design Space (EDS)[21] is a numerical simulation developed by Georgia Tech under the PARTNER project whose development has been sponsored by the FAA. EDS is capable of estimating source noise, exhaust emissions, and performance for potential future aircraft designs under different technological, operational, policy, and market scenarios. While the primary focus of EDS is future aircraft designs (which includes technology modifications to existing aircraft), EDS is capable of analyzing existing aircraft designs (current technology levels), including the simulation of existing aircraft with higher fidelity than is possible using existing noise and emissions tools and inventories. One such output of EDS is aircraft performance characteristics that can be utilized directly in ANOPP.

The Numerical Propulsion System Simulator (NPSS)[22] developed by NASA, is a full propulsion system simulation tool used by aerospace engineers to predict and analyze the aerothermodynamic behavior of commercial jet aircraft, military applications, and space transportation. It is capable of modeling air-breathing propulsion at the system and subsystem level.

ANOPP was employed in the ACRP 02-27 Taxi Noise Project[23]. This project developed a methodology for modeling taxi noise including thrust-noise sensitivities and applied it to generate a database for the full suite of AEDT aircraft for taxi mode (see Figure 4). The database contains spectral directivity (360°) and level information for polar noise sources[24].

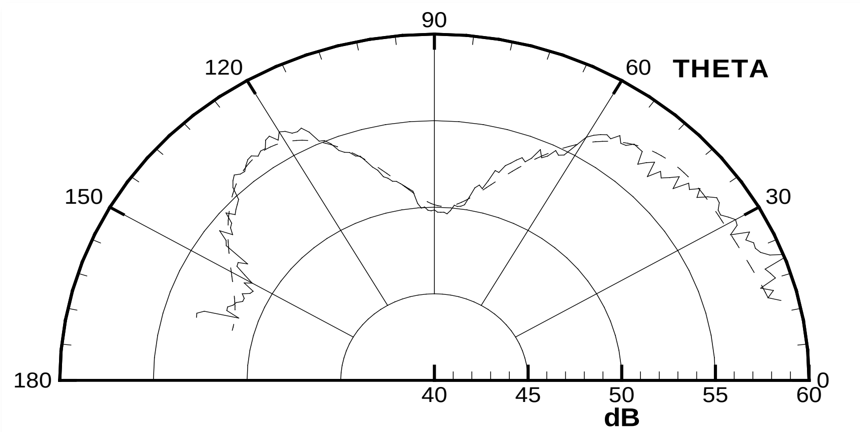

Figure 4. Example Taxi Directivity Data[23]

Another outcome of this project was a process whereby new data can be developed which utilizes a combination of empirical data and first principles modeling results based on ANOPP. Specific engine models built by Georgia Tech under PARTNER using EDS and NASA's Numerical Propulsion System Simulator (NPSS) were adapted and used with ANOPP to model taxi mode and leveraged in the ACRP Taxi project. One of the three processes were applied to each Aircraft in the INM/AEDT database depending on acoustic empirical data availability:

Process I. Empirical Taxi Noise Data and ANOPP data
Process II. Empirical Taxi Noise Data Only
Process III. No Empirical Taxi Noise Data

This current project did not have sufficient scope to model specific aircraft using ANOPP and explore the combination of ANOPP source modeling for in flight modes with other empirical or existing AEDT data, however ACRP 02-27 has demonstrated the feasibility and utility of this approach.

Another project leveraging advanced technology such as ANOPP is the Georgia Tech ASCENT Project 43 "Noise Power Distance Re-evaluation", which utilized ANOPP in conjunction with EDS to develop polar noise sources which include the effects of airframe components such as landing gear, flaps and slats[25]. While this project adapted the existing AEDT NPD structure to select from a collection of alternate NPDs, an artifact of the analysis was the creation of ANOPP polar sources which contain full 3D spectral directivity and were they to be made available, could be used directly as polar sources in AAM modeling to assess the directivity and spectral effects.

2.2.3.2 FLULA2

Directivity data from the Swiss Federal Laboratories for Materials Science and Technology's (EMPA) "Fluglaern" (FLULA2) were also investigated for this analysis[32,33]. The FLULA2 database contains aircraft source directivity patterns for various commercial and military aircraft. These source data are empirically based from flyover noise gathered from an array of microphones near Zurich Airport in 1991 and 1996.

The underlying FLULA2 dataset included one-third octave-band spectral data from 25 Hz to 5,000 Hz adjusted for effects of spherical spreading, atmospheric absorption at standard weather conditions (15°C and 70% relative humidity) and delay time between the source and receiver. The processed data are reconstructed sound source spectral directivity as radiated at some reference radius R around the aircraft for each emission angle Θ, which assumes axisymmetric directivity around the aircraft axis (flight path vector) and uniformly spaced spectra for emission angles in the range 15° to 165° degrees. The final adjusted data are converted to overall A-weighted sound pressure levels (OASPL), and those data are then used to derive coefficients of a polynomial describing the directivity pattern of the aircraft in flight, as a function of propagation distance and emission angle. The database includes both approach and departure data. An example of FLULA2 source directivity for different distances is shown in Figure 5. In FLULA2, these noise data are then adjusted to account for lateral attenuation, terrain effects, non-standard atmospheric effects, velocity effects and power setting differences, as the aircraft travels along the flight path., which is summarized in Figure 6.

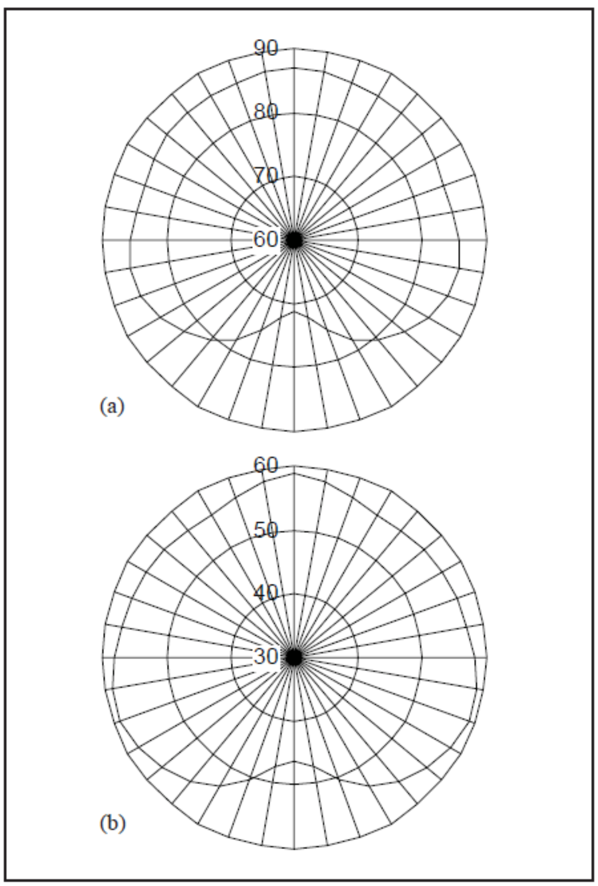

Figure 5. A-weighted Directivity Pattern for A320 "Departure", Equipped with CFM56-5B4-2 for a Medium Takeoff Weight at: (a) r = 305 meters, and (b) and at r = 3000 meters[33]

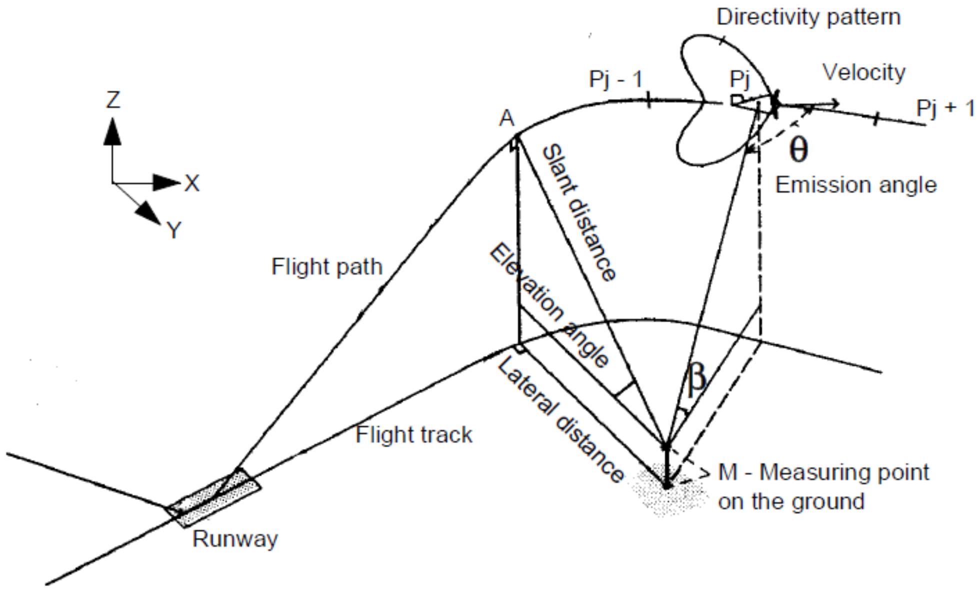

Figure 6. Summary of Flight Path Geometry Components Used for Aircraft Noise Predictions in EMPA's FLULA2[32]

The FLULA2 database is a proprietary database. However, two example directivity data sets are presented in "Sound Source Data for Aircraft Noise Simulation"[33]. These data include the Airbus A320 with CFM56-5B4-2 for a medium take-off weight (less than 85% of the maximum take-off weight), and the McDonnell Douglas DC-9-30 with JT8D-9 for a medium take-off weight (less than 85% of the maximum take-off weight). These example directivities were used for this analysis. The equivalent AEDT aircraft are included in Table 1.

Table 1. List of FLULA2 Example Aircraft and the Equivalent AEDT Aircraft

FLULA 2 Aircraft	Corresponding AEDT Aircraft
A320 with CFM56-5B4-2 engines	A320-211 (with CFM565)
DC9-30 with JT8D-9 engines	DC930 (with 2JT8D)

2.3 Available Data for Polar Source Development

The second task focused on the development of 3-D polar sources using existing data sources (NPDS and spectral classes) and existing methods and tools, although recommendations on future data needs and tools should be developed (such as developing 3-D polar sources from measurement data). This task was not scoped to include a detailed investigation of different methods of developing 3-D polar sources from a range of fidelity of measurement data, nor the blending of different data sources and methods using hybrid analytical-empirical techniques (such as combining NPDs, measurements, ANOPP, etc.) to develop a single 3-D polar source. However, when data and methods were easily available, they were leveraged in the analysis. This is primarily a feasibility study that will result in the development of 3-D polar sources for several example fixed wing aircraft, utilizing and fine-tuning the recommended methods from the first task.

For this effort, several fixed-wing aircraft data sources were identified and used to develop 3-D polar sources. Two types of sources were required to develop polar spheres: spectral data and directivity data.

Spectral data are already included in the AEDT database in the form of spectral classes, which are readily available, and are widely accepted and utilized in AEDT[1]. Since AEDT spectral classes are often normalized, they can then be calibrated to the aircraft-specific NPD data at 1000 ft for the corresponding thrust setting. In addition, each aircraft data submitted by airframe manufacturers for AEDT or INM since the early 2000s has included aircraft-specific spectral data, for use in the spectral class assignment process. These aircraft-specific spectra provided a second spectral data source for this analysis. Since this effort was a proof of concept, no additional spectral data sources were investigated.

A wider range of directivity data sources were utilized for this effort. As a baseline case, omnidirectional directivity was used, which assumes uniform directivity over the source. In the current release of AEDT (AEDT 2c), a directivity curve is provided that represents the noise directivity around a jet aircraft during the start-of-takeoff-roll (SOTR)[1]. While this directivity may not be perfectly representative of jet noise directivity during flight, it does adequately characterize a forward flight jet noise cardioid shape and is a widely-accepted and empirically based aircraft noise directivity adjustment, and was therefore utilized in this study as a readily available directivity data source. An updated start-of-takeoff-roll directivity based on SAE-AIR-6297[5] is slated to be added to a future release of AEDT (possibly the AEDT 3 series) and is based on a more current aircraft fleet, so it was also identified as a directivity data source. Since the SAE-AIR-6297 methodology provides both jet and turboprop directivity curves, the jet directivity curve was used for this analysis (see Figure 2). As mentioned in Section 2.2.3, EMPA developed detailed distance-based directivity curves for a range of different aircraft, two of which have publically-available example implementations and were also identified as limited directivity data source. Finally, detailed aircraft-specific aircraft start-of-takeoff-roll directivity data were collected as part of the Washington Dulles International Airport study[34], which were used to develop the SAE-AIR-6297 directivity curves. Although these directivity curves were non-symmetric, the left and right halves of the curves were used as separately to create symmetrical directivity sources. For example, a mirror image of the right side directivity was implemented as the left side directivity, and the end result was a symmetrical directivity based on the right-side data only.

These spectra and directivity data could be combined into 12 different types of polar sources for each aircraft type. Given the range of data sources, polar sources of different fidelity were developed. They range from aircraft generic (spectral class and omnidirectional or SOTR directivity) to aircraft-specific (data submittal spectra and EMPA or Dulles directivity). The different polar sources utilized in this analysis are presented in Figure 7 and Figure 8 for the DC9-4, and Figure 9 and Figure 10 for the 767-400.

Polar Source Analysis

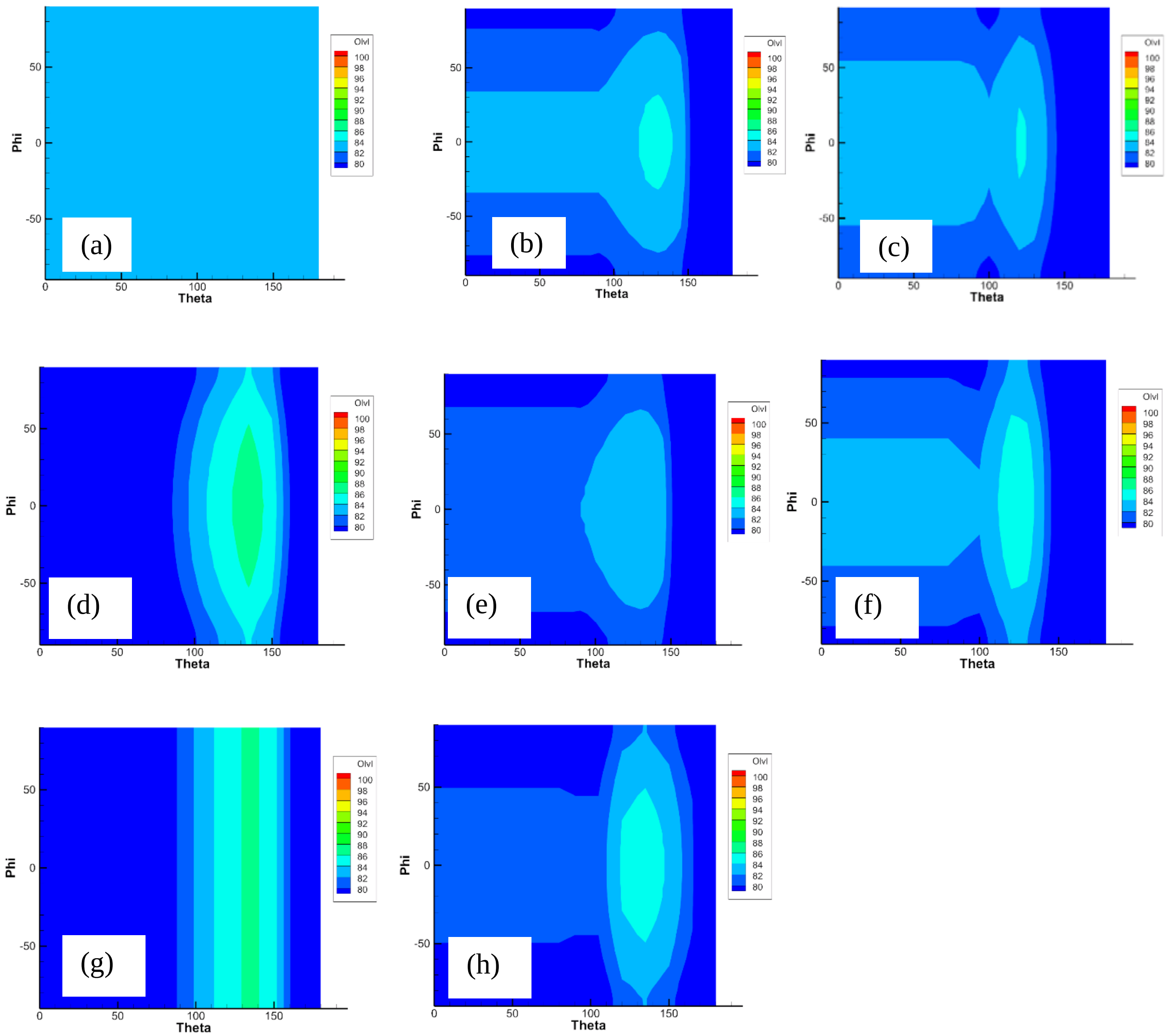

Figure 7. DC9-4 Approach Polar Sources Used in the Phase 1 Analysis: (a) Spectral Class Data and Omnidirectional Directivity, (b) Spectral Class Data and AEDT2 SOTR Directivity, (c) Spectral Class Data and AEDT3 JET SOTR Directivity, (d) Spectral Class Data and EMPA Directivity, (e) Data Submittal Spectrum and AEDT2 SOTR Directivity, (f) Data Submittal Spectrum and AEDT3 JET SOTR Directivity (g) Data Submittal Spectrum and EMPA Directivity, and (h) Data Submittal Spectrum and Dulles Left Directivity

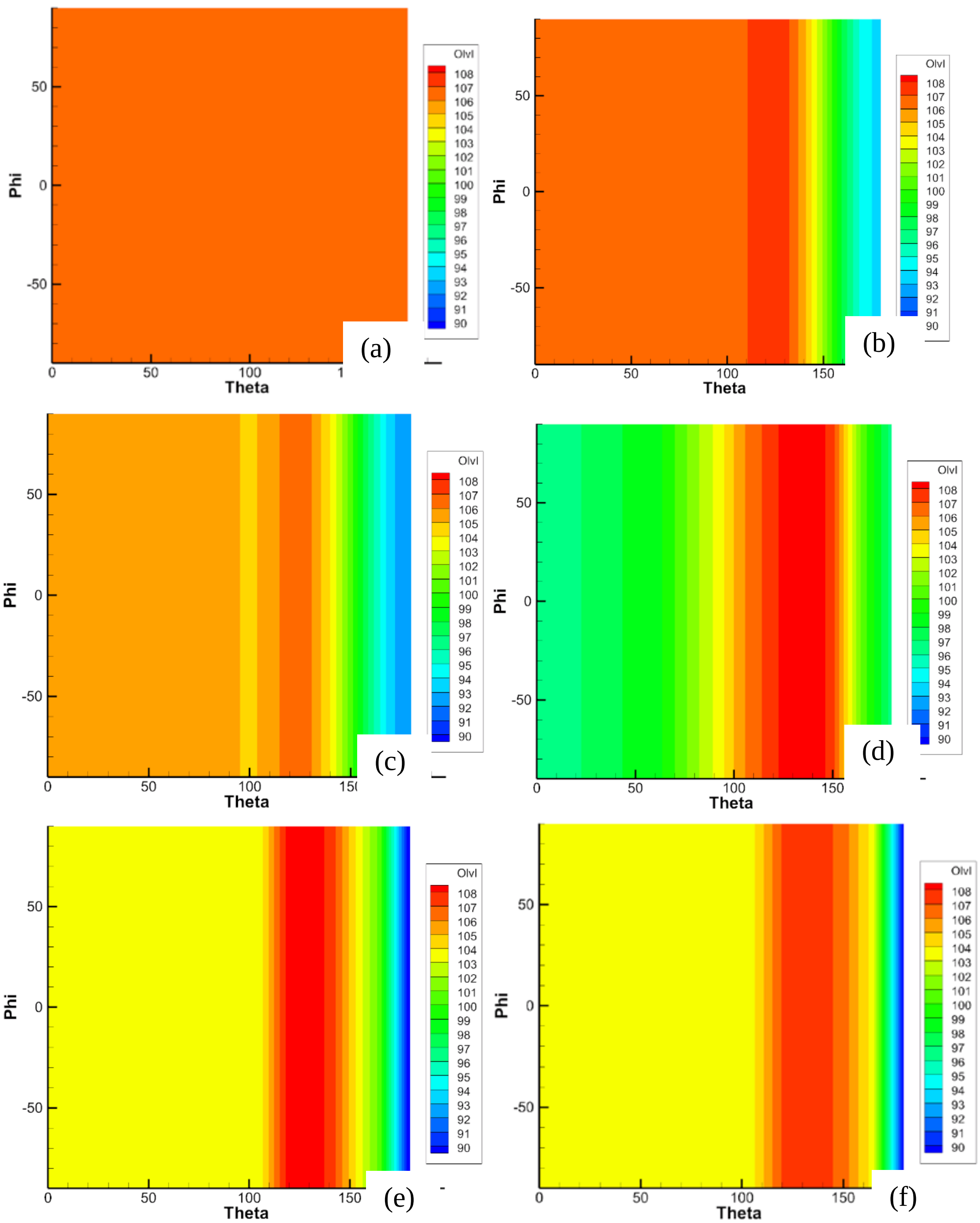

Figure 8. DC9-4 Departure Polar Sources Used in the Phase 2 Analysis: (a) Spectral Class Data and Omnidirectional Directivity, (b) Spectral Class Data and AEDT3 JET SOTR Directivity, (c) Data Submittal Spectrum and AEDT3 JET SOTR Directivity, (d) Data Submittal Spectrum and EMPA Directivity, (e) Data Submittal Spectrum and Dulles Right Directivity, and (f) Data Submittal Spectrum and Dulles Left Directivity

Polar Source Analysis

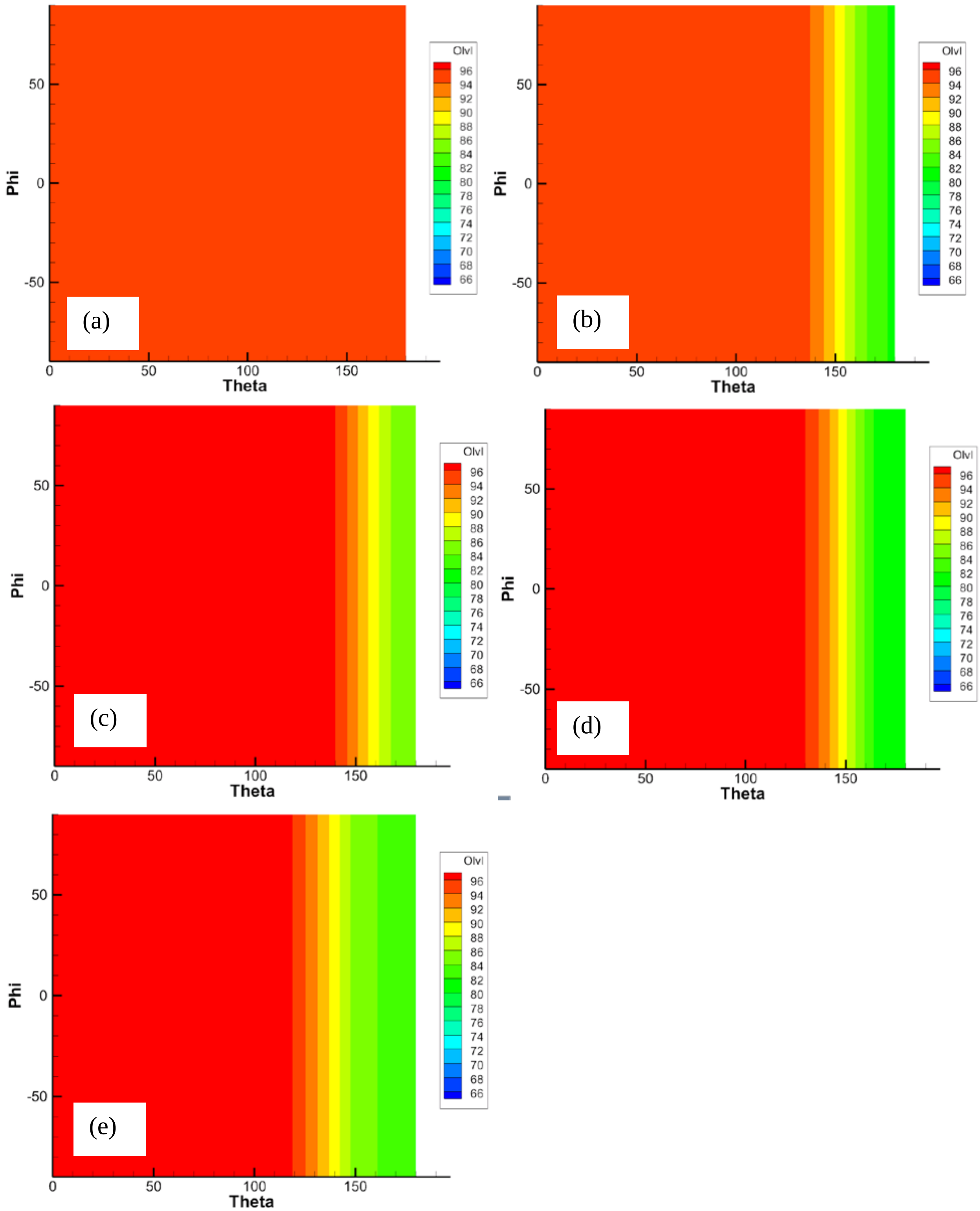

Figure 9. 767-400 Departure Polar Sources Used in the Phase 2 Analysis: (a) Spectral Class Data and Omnidirectional Directivity, (b) Spectral Class Data and AEDT3 JET SOTR Directivity, (c) Data Submittal Spectrum and AEDT3 JET SOTR Directivity, (d) Data Submittal Spectrum and Dulles Right Directivity, and (e) Data Submittal Spectrum and Dulles Left Directivity

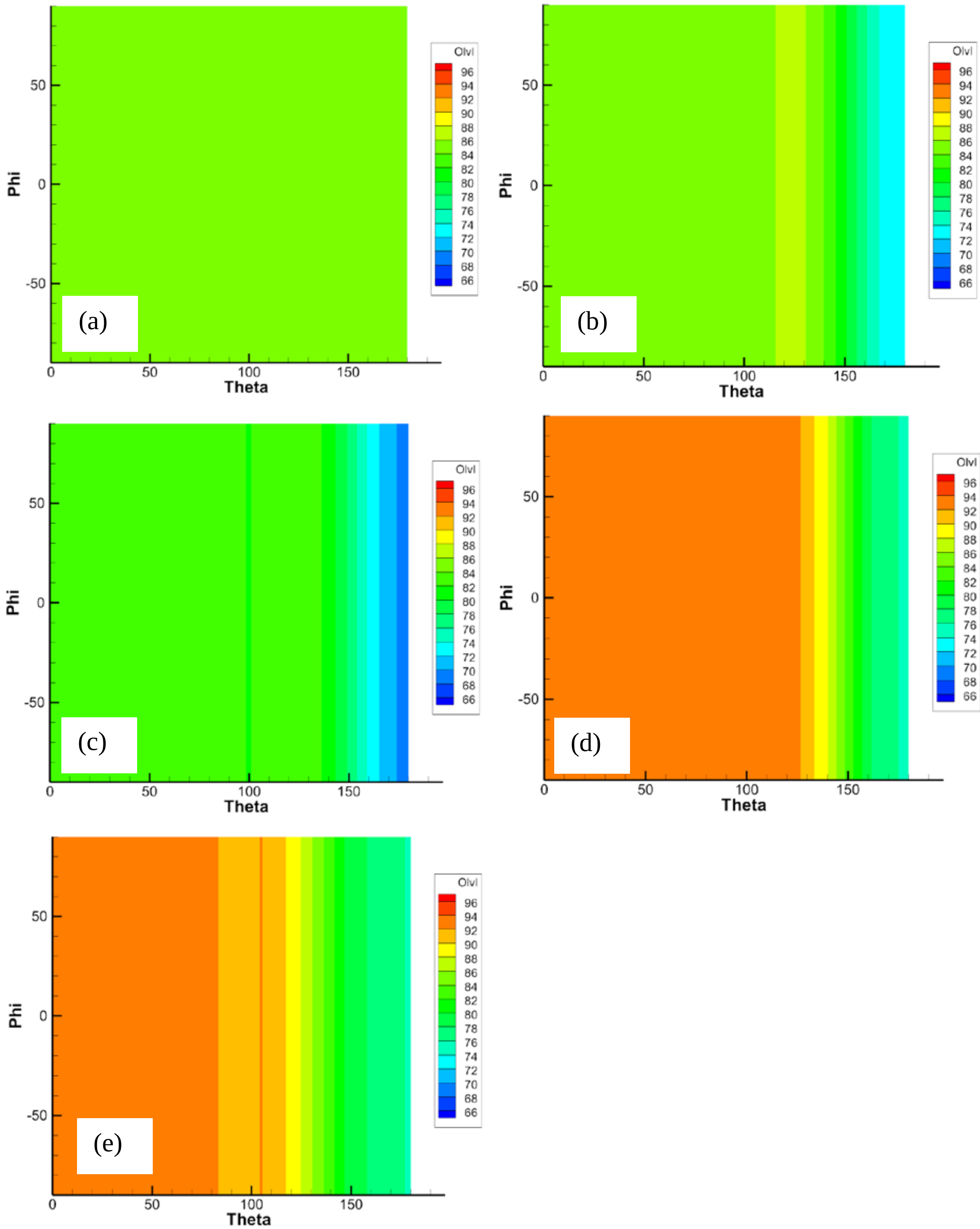

Figure 10. 767-400 Approach Polar Sources Used in the Phase 2 Analysis: (a) Spectral Class Data and Omnidirectional Directivity, (b) Spectral Class Data and AEDT3 JET SOTR Directivity, (c) Data Submittal Spectrum and AEDT3 JET SOTR Directivity, (d) Data Submittal Spectrum and Dulles Right Directivity, and (e) Data Submittal Spectrum and Dulles Left Directivity

3 Polar Source Comparison

The polar source comparison consisted of four sub-tasks: a description of the modeling tools used for the comparison, an overview of the polar source development process, a description of the test study, the test matrix, and the source normalization procedure.

3.1 Modeling Tools and Validation data

Since AEDT and AEDT-Ray do not currently accept 3-D polar sources, external tools will be utilized for this comparison and validation. The comparison testing was conducted with NASA's AAM V1[27]. AAM was chosen because it was a known and validated noise model that accepted polar sources. Some existing polar sources have already been developed for use with AAM, and the publically-available polar sources may be considered for future analyses.

The comparison testing included AAM studies meant to replicate an existing data set for validation purposes. Data from a 2000 flight test at NASA's Wallops Flight Facility was chosen for this purpose[15]. The joint NASA and Volpe measurements were conducted to investigate the accuracy of the lateral attenuation algorithm in SAE-AIR-1751[28], and eventually was used to develop an update to that guidance document: SAE-AIR-5662[5]. This data set was chosen because it was a known data set from a controlled flight test with noise, atmospheric and tracking data†, the data set included four different aircraft performing approach and departure operations, and the noise data were collected at a range of locations lateral to the flight path. In addition, some existing polar sources have already been developed from the Wallops data, and they may be considered for future analyses.

3.2 Polar Source Development

This review supplemented the aircraft source method review included in the draft white paper "Acoustics Modeling in AEDT: Long Term Vision and Development Roadmap"[29]. Since a wide range of aircraft source data exists with varying data quality, this effort looked at the development of a series of 3-D polar sources for each aircraft covering a range of data fidelity, including, but not limited to:

- Basic fidelity source: an omnidirectional 3-D polar source developed from NPDs and spectral classes,
- Moderate fidelity source: a higher fidelity 3-D polar source developed from NPDs, spectral classes, directivity data, and other AEDT-based directivity adjustments, and
- High fidelity source: a 3-D polar source developed from detailed noise data from detailed source noise measurements (based on available data).

In order to develop Basic and Moderate fidelity sources, an in-house Fortran tool call SphereBuilder was constructed to analytically create polar sources for use with the Advanced Acoustic Model

† Note: Although simplified atmospheric conditions were modeled, winds were not modeled.

(AAM)[27,31]. This tool facilitates analysis of different directivity patterns and spectral data and incorporates the effects of Doppler frequency shifting. The resultant noise sphere set can be utilized to assess different directivity and spectral assumptions on noise results (levels, time histories, and contours) for specific flight operations. The tool is keyword driven and each feature is described in Appendix 9.1.

3.2.1 Development of Polar Noise Sources from Flight Test Measurement Data

Development of High fidelity noise sources for the B767 and DC9 leveraged the Wallops measurements[26]. This process requires empirical data and use of the Acoustic Re-propagation Technique (ART)[‡] process (developed as part of the NASA-AAM tool suite) in conjunction with an open source, platform-independent database[35], a robust noise source can be constructed that is well suited for use in simulation noise models using a widely applicable methodology for creating a three dimensional noise source from measurements that can account for spectral source directivity[36]. Others have adopted similar procedures for obtaining polar noise source data from measurements[33,37] and for expanding/enhancing existing simplified data with limited measurement data availability[38].

Polar sources may contain a variety of noise data (one-third octave band, narrow-band or pure tone and phase or pressure as a function of time) representing the source at a fixed distance for all spherical angles. Such noise spheres can be combined to represent complex noise sources to accurately predict the near and far field noise environments.

Figure 11 shows the first step of the ART process. In order to characterize a dynamic noise source, such as the helicopter depicted in the figure, one need only understand that for a given moment in time, the sound emitted from it can be recorded at some later time by a microphone array. Attenuation due to physical aspects such as spherical spreading, atmospheric absorption, and ground effects, can be determined with a capable environmental noise model. These attenuation calculations are not the focus of ART. The focus of ART is to establish the geometric relationship between the source and each microphone at all discrete times. This allows the frame of reference to change from an earth-fixed coordinate system as in Figure 11a to a source-fixed system depicted in Figure 11b, and permits the subtraction of the propagation effects from the recorded sound (re-propagation) so that the resulting data may be represented on a sphere. This polar description may be used to represent the source in a noise model for the operating state in which it was operating during the recording. This calls for the source to operate in a ‘steady state’ throughout the measurement. A discrete set of polar sources is created to span the range of a vehicle’s operating envelope intended for modeling.

‡ The ART software is part of the Advanced Acoustic Model Toolset and has been developed to work in conjunction with the propagation piece computed using AAM and the microphone data adjustments and sphere assembly calculations handled by ART. The result is a binary NetCDF format platform-independent file which represents a compact source three-dimensional spectral noise emission. Within the AAM ART standard definition, atmospheric absorption and propagation effects are removed back to the compact source center while spherical spreading is based on the reference sphere radius.

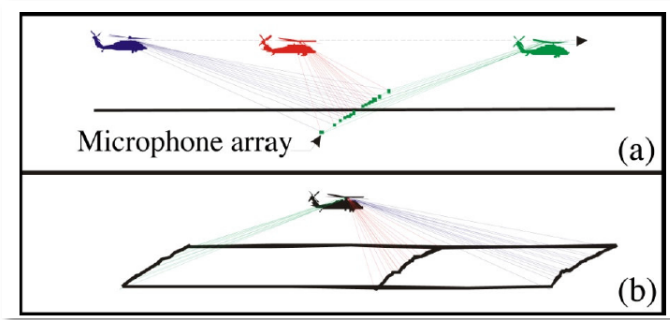

Figure 11. Graphical representation of noise emission from a moving vehicle in (a) Earth-based and (b) vehicle-based reference systems.[36]

It is important to note that although High fidelity polar sources were identified for this analysis, they were not included in the comparison testing, because the same data from the Wallops study were used for validation.

3.3 Test Study Description

The AAM test studies were based on the Wallops flight test[19]. This flight test included approach and departure events for the Boeing 767-400, the McDonnell Douglas DC-9-4, the Dassault Falcon 2000 and the Beechcraft King Air. For this analysis, the 767-400 and the DC9-4 were modeled. A range of flight conditions were flown during the flight test, which are described in Table 2. These flight conditions were flown through a u-shaped microphone array. This comparison focused on modeling receptors that corresponded to the horizontal portion of the microphone array: microphones 6 through 15 (see Table 3). These included nine pole microphones (24 ft above ground level) and one ground plane microphone. Figure 12 shows example flight tracks in relation to those microphone locations.

Table 2. Flight Conditions from the Wallops Flight Test

Configuration Series	Description	Aircraft Modeled	Comparison Test
100	Full power with takeoff flaps, accelerating	DC9-4, 767400	Phase 2
200	De-rate power with takeoff flaps, accelerating	-	-
300	Low power with approach flaps, constant speed	767400	Phase 2
400	Low power with flaps retracted, constant speed	DC9-4	Phase 1

Table 3. Microphone Locations for the Wallops Flight Test

Microphone Number	Microphone Type	X (feet)	Y (feet)	Z (feet AGL)
1	Vertical Array	0	-425	200
2	Vertical Array	0	-425	162
3	Vertical Array	0	-425	125
4	Vertical Array	0	-425	86
5	Vertical Array	0	-425	45
6	Pole	0	-294	24
7	Pole	0	-203	24
8	Pole	0	-143	24
9	Pole	0	-98	24
10	Ground Board	0	0	0
11	Pole	0	0	24
12	Pole	0	98	24
13	Pole	0	143	24
14	Pole	0	203	24
15	Pole	0	294	24
16	Vertical Array	0	425	45
17	Vertical Array	0	425	86
18	Vertical Array	0	425	125
19	Vertical Array	0	425	162
20	Vertical Array	0	425	200

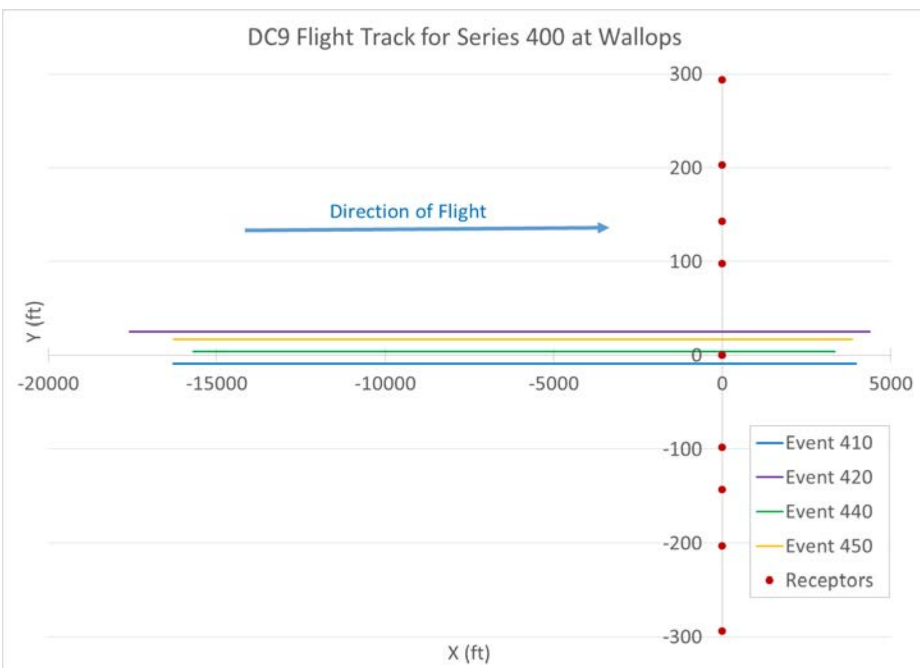

Figure 12. Example Flight Tracks and Relative Microphone Locations from the Wallops Flight Test

3.4 Test Matrix

The comparison testing consisted of two phases. Phase 1 focused on the DC9-4 aircraft flying level at an approach power setting using a clean flaps configuration (Wallops 400 series). Phase 1 reflected a noise source, configuration and operations that were represented by a wide range of data sources and in the Wallops data set. The Phase 1 test matrix includes:

1. DC9-4 approach with a polar source developed using spectral class data and omnidirectional directivity,
2. DC9-4 approach with a polar source developed using spectral class data and the AEDT2 SOTR directivity,
3. DC9-4 approach with a polar source developed using spectral class data and the AEDT3 JET SOTR directivity,
4. DC9-4 approach with a polar source developed using spectral class data and EMPA directivity
5. DC9-4 approach with a polar source developed using the data submittal spectrum and the AEDT2 SOTR directivity,
6. DC9-4 approach with a polar source developed using the data submittal spectrum and the AEDT3 JET SOTR directivity,
7. DC9-4 approach with a polar source developed using the data submittal spectrum and EMPA directivity, and
8. DC9-4 approach with a polar source developed using the data submittal spectrum and the Dulles directivity for the DC9 (using left side directivity only).

The test matrix for Phase 1 is summarized in Table 4. This test matrix was repeated for the four events in the 400 series of the Wallops data set (events 410, 420, 440 and 450). This resulted in 32 AAM runs. The AEDT aircraft used for the source in Phase 1 was the DC930. A-weighted maximum sound pressure levels (LAMAX) were compared as part of Phase 1 testing.

Table 4. Phase 1 Test Matrix: DC9-4 Wallops 400 Series

	Spectral Data Source	
Directivity	**Spectral Class**	**Data Submittal**
Omni	Y	
AEDT2 SOTR	Y	Y
AEDT3 Jet SOTR	Y	Y
EMPA	Y	Y
Dulles - Left		Y
Dulles - Right		

Phase 2 focused on events that were more reflective of common aircraft operations that may benefit from the additional directivity provided by polar sources. This included the DC9-4 aircraft flying at a departure power setting using a takeoff flaps configuration (Wallops 100 series), the 747-400 flying the same series (Wallops 100 series) and at an approach power setting using approach flaps configuration (Wallops 300 series). The test matrix was reduced for Phase 2 testing in order to focus on the most promising polar source data sets, and to maximum the amount of testing that could be done given the project schedule and funds. The Phase 2 test matrix includes:

1. DC9-4 departure with a polar source developed using spectral class data and omnidirectional directivity,
2. DC9-4 departure with a polar source developed using spectral class data and the AEDT3 JET SOTR directivity,
3. DC9-4 departure with a polar source developed using the data submittal spectrum and the AEDT3 JET SOTR directivity,
4. DC9-4 departure with a polar source developed using the data submittal spectrum and EMPA directivity
5. DC9-4 departure with a polar source developed using the data submittal spectrum and the Dulles directivity for the DC9 (using left side directivity only),
6. DC9-4 departure with a polar source developed using the data submittal spectrum and the Dulles directivity for the DC9 (using right side directivity only),
7. 767-400 departure with a polar source developed using spectral class data and omnidirectional directivity,
8. 767-400 departure with a polar source developed using spectral class data and the AEDT3 JET SOTR directivity,
9. 767-400 departure with a polar source developed using the data submittal spectrum and the AEDT3 JET SOTR directivity,
10. 767-400 departure with a polar source developed using the data submittal spectrum and the Dulles directivity (using left side directivity only),
11. 767-400 departure with a polar source developed using the data submittal spectrum and the Dulles directivity (using right side directivity only),
12. 767-400 approach with a polar source developed using spectral class data and omnidirectional directivity,
13. 767-400 approach with a polar source developed using spectral class data and the AEDT3 JET SOTR directivity,
14. 767-400 approach with a polar source developed using the data submittal spectrum and the AEDT3 JET SOTR directivity,
15. 767-400 approach with a polar source developed using the data submittal spectrum and the Dulles directivity (using left side directivity only), and
16. 767-400 approach with a polar source developed using the data submittal spectrum and the Dulles directivity (using right side directivity only).

The test matrix for Phase 2 is summarized in Table 5. This test matrix was repeated for the five events in the 100 series for the DC9-4 (events 110, 120, 130, 140 and 150), the seven events in the 100 series for the 767-400 (events 110, 112, 120, 121, 140, 150 and 160), and the sic events in the 300 series for the 767-400 in the Wallops data set (events 310, 321, 330, 340, 350 and 360). This resulted in 95 AAM runs. The AEDT aircraft used for the sources in Phase 2 were the DC930 and 767400. A-weighted sound exposure levels (SEL) were compared as part of Phase 2 testing, since SEL is used to compute the day-night level (DNL) noise metric used in airport noise analyses.

Table 5. Phase 2 Test Matrix: DC9-4 Wallops 100 Series, and 767-400 Wallops 100 and 300 Series

	DC9-4 departure (full power takeoff flaps, accelerating - based on Wallops 100 series)		767-400 departure (full power takeoff flaps, accelerating - based on Wallops 100 series)		767-400 approach (low power with flaps, constant speed - based on Wallops 300 series)	
Directivity	**Spectral Class**	**Data Submittal**	**Spectral Class**	**Data Submittal**	**Spectral Class**	**Data Submittal**
Omni	Y		Y		Y	
AEDT2 SOTR						
AEDT3 Jet SOTR	Y	Y	Y	Y	Y	Y
EMPA		Y				
Dulles - Left		Y		Y		Y
Dulles - Right		Y		Y		Y

3.5 Source Normalization

To be sure that the polar source sphere noise levels are consistent with the corresponding NPD noise and thrust levels, each sphere was calibrated using the 1000 ft. overflight LAMAX NPD level for the appropriate thrust setting (which is determined by the aircraft flight series and trajectory data). An artificial calibration AAM run was created to model the noise, specifically LAMAX, from the spheres at the 1000 ft. overflight location. The difference in LAMAX level between the NPD and the polar source sphere was applied to the original sphere as a calibration offset. The final calibrated spheres are what is used for the modeling comparisons to the Wallops measured noise data. The tables below summarize the polar source spheres, the associate 1000 ft. overflight LAMAX levels, and the corresponding adjustment, which is the difference between the overflight LAMAX value and the 1000 ft. NPD value for the matching aircraft type and thrust setting.

Table 6 - Calibration Adjustment values for Original DC9 Spheres

Sphere Description	**Spectral Class - Omni**	**Spectral Class - SOTR**	**DataSub - SOTR**	**DataSub - EMPA**	**DataSub - DullesL**	**DataSub - DullesR**
Sphere name	DC9SC001	DC9SC002	DC9SS001	DC9SS002	D9SL003	D9SR003
1000 ft. LAMAX (dB)	90.2	89.6	105.0	114.0	106.8	107.3
Adjustment value (dB)	20.3	20.9	5.5	-3.5	3.7	3.2

Table 7 - Calibration Adjustment values for Original 767-400 Departure condition Spheres

	DEP				
Sphere Description	**Spectral Class - Omni**	**Spectral Class - SOTR**	**DataSub - SOTR**	**DataSub - DullesL**	**DataSub - DullesR**
Sphere name	767CD001	767CD002	767SD001	767DL002	767DR002
1000 ft. LAMAX (dB)	89.3	88.7	102.9	101.4	102.7
Adjustment value (dB)	11.5	12.1	-2.1	-0.6	-1.9

Table 8 - Calibration Adjustment values for Original 767-400 Arrival condition Spheres

	ARR				
Sphere Description	**Spectral Class - Omni**	**Spectral Class- SOTR**	**DataSub - SOTR**	**DataSub - Dulles L**	**DataSub - Dulles R**
Sphere name	767CA001	767CA002	767SA001	767AL002	767AR002
1000 ft. LAMAX (dB)	89.2	88.7	98.5	97	98.2
Adjustment value (dB)	0.9	1.4	-10	-8.5	-9.7

After running the first series of comparison tests between the measured Wallops data and the polar source AAM results, it became clear that there is a relatively consistent offset between the two data sets. Overall, the polar source data was anywhere from 1-4 dB higher than the measured Wallops noise data at all points of interest (POIs), after including the polar source calibration adjustments. This discrepancy was investigated and determined to not be caused by incorrect or mismatched units, noise duration differences, or receiver (POI) locations. In order to make a more direct comparison of the aircraft noise levels for each run, the polar source results were normalized to match the Wallops measured noise levels at the centerline pole microphone location.

The difference in noise level between these two points was calculated, and then applied as an offset to all of the other POI locations for the specific run and directivity combination. This allows for a more direct comparison of the “shape” of the noise results. Most of the discrepancies in shape happen at the outer lateral mic positions, where the measured Wallops data does not always follow the same downward trend as the sphere results. The same type of comparison is difficult to make between the sphere results and the noise cert levels because the sphere results were calibrated based on LAMAX/SEL noise levels as opposed to the final EPNL values. That being said, on first pass, the centerline EPNL values for Takeoff and Approach for the 767-400, as well as the centerline ENPL values for the DC9 Takeoff look to be in agreement with the FAA certification levels.

It is important to note that source calibration procedures are tied to propagation models. Therefore, the final, appropriate source propagation procedure will not be implemented in AEDT until 3-D polar sources are integrated with a propagation model.

4 Modeling Results and Analysis

In this analysis, the modeled results are compared against the equivalent measured results from the Wallops study. Phase 1 focused on clean configuration approach events for a single aircraft represented in all of the data sets being investigated (DC9-4) and the resulting LAMAX noise levels, in order review the proof of concept and flesh out the rest of the test matrix. Phase 2 focused on flying various operations with several aircraft (DC9-4 and 77-400 departures and approaches) and the resulting SEL noise levels, in order to show that the sources may be used for realistic airport operations and for noise metrics that are reflected in FAA noise guidance[§]. These analyses were supplemented by a contour comparison, to show the effects of polar sources on a noise footprint.

4.1 Phase 1 Results Summary

In the Phase 1 testing, the Wallops Series 400 events (approach power with clean configuration) were modeled for the DC9-4. The difference between the measured and modeled LAMAX results for each measurement location (point of interest, or POI) are presented in Table 9 and Table 10. Event-based results are presented in Section 9.2. It is important to note that the Phase 1 testing did not utilize normalized sources.

Table 9. Phase 1 Results: Average Difference between Measured and Modeled Results for the DC9-4 Wallops Series 400 (difference in dB LAMAX for each POI)

POI	SC-Omni	SC-SOTR (AEDT 2)	SC-SOTR (AEDT 3)	SC-EMPA	DataSub-SOTR (AEDT 2)	DataSub-SOTR (AEDT 3)	DataSub-EMPA	DataSub-Dulles (Left)
6	-0.6	0.0	0.0	-0.8	-0.5	-0.5	-2.4	-0.2
7	-0.8	-0.6	-0.5	-1.6	-1.1	-1.1	-2.9	-1.0
8	-0.3	-0.3	-0.2	-1.6	-1.0	-0.8	-2.7	-0.9
9	0.9	0.6	0.7	-0.9	0.0	0.1	-1.8	0.0
10	-0.6	-1.1	-1.0	-2.5	-1.5	-1.5	-3.0	-1.5
11	1.1	0.6	0.6	-0.9	0.0	-0.1	-1.6	-0.1
12	1.8	1.4	1.5	0.0	0.8	0.8	-0.8	0.8
13	0.2	0.1	0.1	-1.4	-0.5	-0.4	-2.4	-0.6
14	0.3	0.3	0.5	-0.8	-0.2	-0.1	-2.0	-0.2
15	0.3	0.8	0.8	0.0	0.3	0.3	-1.6	0.5
16	0.2	0.2	0.3	-1.1	-0.4	-0.3	-2.1	-0.3
Mean	**0.2**	**0.2**	**0.3**	**-1.1**	**-0.4**	**-0.3**	**-2.1**	**-0.3**

§ SEL is used to compute DNL, which is utilized frequently in noise impact analyses.

Polar Source Analysis

Table 10. Phase 1 Results: Standard Deviation of Difference between Measured and Modeled Results for the DC9-4 Wallops Series 400 (difference in dB LAMAX for each POI)

POI	SC-Omni	SC-SOTR (AEDT 2)	SC-SOTR (AEDT 3)	SC-EMPA	DataSub-SOTR (AEDT 2)	DataSub-SOTR (AEDT 3)	DataSub-EMPA	DataSub-Dulles (Left)
6	0.9	0.5	0.9	1.1	0.6	0.8	1.0	1.3
7	0.8	1.1	1.4	1.6	1.0	1.4	1.2	1.6
8	1.0	1.0	1.4	1.3	0.9	1.4	1.0	1.5
9	1.4	1.3	1.7	1.2	1.2	1.6	0.9	1.4
10	1.7	1.6	1.7	0.9	1.6	1.7	0.8	1.1
11	1.8	1.7	1.8	1.2	1.7	1.8	1.1	1.3
12	1.5	1.2	1.6	1.1	1.2	1.5	0.9	1.3
13	1.4	1.0	1.5	1.2	0.9	1.4	1.1	1.4
14	0.9	0.7	1.1	1.1	0.6	1.1	0.8	1.2
15	0.6	0.7	0.9	1.4	0.6	0.9	1.2	1.5
16	1.0	0.9	1.2	1.0	0.8	1.2	0.7	1.2
Mean stdev	**1.2**	**1.1**	**1.4**	**1.2**	**1.0**	**1.3**	**1.0**	**1.3**

When averaged across all events, most polar sources yielded similar results for the DC9-4 Wallops Series 400 scenario, except for the sources that used EMPA directivity, which showed an offset of approximately 2 dB.

Since comparison of measurement and modeled data did identify a preferred polar source, the results were also evaluated as event averages across all the microphone positions (see Table 11 and Table 12).

Table 11. Phase 1 Results: Average Difference between Measured and Modeled Results for the DC9-4 Wallops Series 400 (difference in dB LAMAX for each Event)

Event	SC-Omni	SC-SOTR (AEDT 2)	SC-SOTR (AEDT 3)	SC-EMPA	DataSub-SOTR (AEDT 2)	DataSub-SOTR (AEDT 3)	DataSub-EMPA	DataSub-Dulles (Left)
410	-1.1	-0.7	-1.4	-2.4	-1.2	-1.9	-3.1	-1.8
420	0.2	-0.5	-0.3	-1.5	-1.0	-0.8	-2.2	-0.8
440	-0.1	0.4	0.8	0.4	-0.3	0.1	-1.1	1.4
450	1.8	1.5	1.9	-0.7	0.9	1.3	-2.1	0.0
Mean	**0.2**	**0.2**	**0.3**	**-1.1**	**-0.4**	**-0.3**	**-2.1**	**-0.3**
Stdev of Mean	**1.05**	**0.86**	**1.22**	**1.02**	**0.81**	**1.17**	**0.72**	**1.17**

Table 12. Phase 1 Results: Standard Deviation of Difference between Measured and Modeled Results for the DC9-4 Wallops Series 400 (difference in dB LAMAX for each Event)

Event	SC-Omni	SC-SOTR (AEDT 2)	SC-SOTR (AEDT 3)	SC-EMPA	DataSub-SOTR (AEDT 2)	DataSub-SOTR (AEDT 3)	DataSub-EMPA	DataSub-Dulles (Left)
410	0.57	0.56	0.56	0.57	0.53	0.57	0.59	0.56
420	1.16	1.21	1.18	1.23	1.20	1.20	1.16	1.29
440	0.89	1.02	0.99	1.17	1.01	0.98	0.86	0.96
450	1.49	1.14	1.20	0.83	1.11	1.14	1.14	0.90
Mean of Stdev	**1.03**	**0.98**	**0.98**	**0.95**	**0.96**	**0.97**	**0.94**	**0.93**
Max Stdev	**1.49**	**1.21**	**1.20**	**1.23**	**1.20**	**1.20**	**1.16**	**1.29**

When considering the average difference between each polar source and the corresponding measurement data for each DC9-4 Wallops 400 series event, the polar source generated using the AEDT spectral class and the start-of-takeoff-roll directivity found in AEDT 2c performed slightly better than the other polar sources. However, since these results showed the SAE-AIR-1845 (in AEDT 2c) and the SAE-AIR-6297 (scoped for AEDT 3) behind-start-of-takeoff-roll directivity yielding very similar results, and since the SAE-AIR-6297 will eventually replace the SAE-AIR-1845 directivity in AEDT, the sources with the SAE-AIR-1845 (AEDT2) directivity were not included in Phase 2 of this analysis. Phase 1 also showed the importance of data normalization for this analysis.

4.2 Phase 2 Results Summary

In the Phase 2 testing, the Wallops Series 400 events (approach power with clean configuration) were modeled for the DC9-4. The difference between the measured and modeled LAMAX results for each measurement location (point of interest, or POI) are presented in Table 13 through Table 18. Event-based results are presented in Section 9.3. Based on the experience gain during Phase 1, the Phase 2 source data were normalized as discussed in Section 3.5. It should be noted that the 767-400 was not included in the publically-available FLULA2 data set, so only the DC9-4 events were modeled using the EMPA directivity.

Table 13. Phase 2 Results: Average Difference between Measured and Modeled Results for the DC9-4 Wallops Series 100 (difference in dB SEL for each POI)

POI	SC-Omni	SC-SOTR	DataSub-SOTR	DataSub-EMPA	DataSub-Dulles (Left)	DataSub-Dulles (Right)
6	0.3	0.3	0.2	0.3	0.3	0.3
7	0.6	0.5	0.5	0.6	0.6	0.5
8	0.4	0.4	0.3	0.4	0.3	0.4
9	-0.6	-0.6	-0.6	-0.7	-0.6	-0.6
10	-0.3	-0.2	-0.2	-0.3	-0.3	-0.2
11	0.0	0.0	0.0	-0.2	0.0	0.0
12	-0.5	-0.5	-0.5	-0.6	-0.5	-0.5
13	0.9	0.9	0.8	0.8	0.8	0.8
14	0.5	0.5	0.5	0.6	0.5	0.5
15	0.1	0.0	0.0	0.1	0.1	0.1
16	0.3	0.3	0.0	0.5	0.4	0.4
Mean	**0.2**	**0.1**	**0.1**	**0.1**	**0.1**	**0.1**

Table 14. Phase 2 Results: Standard Deviation of Difference between Measured and Modeled Results for the DC9-4 Wallops Series 100 (difference in dB SEL for each POI)

POI	SC-Omni	SC-SOTR	DataSub-SOTR	DataSub-EMPA	DataSub-Dulles (Left)	DataSub-Dulles (Right)
6	0.5	0.6	0.5	1.1	0.6	1.0
7	0.1	0.3	0.3	0.8	0.4	1.0
8	0.1	0.2	0.2	0.6	0.3	0.8
9	0.3	0.3	0.3	0.8	0.4	0.6
10	0.1	0.1	0.1	0.5	0.1	0.4
11	0.0	0.0	0.0	0.3	0.0	0.0
12	0.3	0.3	0.2	0.7	0.3	0.5
13	0.1	0.3	0.3	0.7	0.4	0.9
14	0.2	0.5	0.5	0.9	0.6	1.1
15	0.3	0.5	0.5	0.8	0.6	1.0
16	0.4	0.5	0.8	0.9	0.6	1.1
Mean stdev	**0.2**	**0.3**	**0.3**	**0.7**	**0.4**	**0.8**

Polar Source Analysis

Table 15. Phase 2 Results: Average Difference between Measured and Modeled Results for the 767-400 Wallops Series 100 (difference in dB SEL for each POI)

POI	SC-Omni	SC-SOTR	DataSub-SOTR	DataSub-Dulles (Left)	DataSub-Dulles (Right)
6	-0.1	0.0	0.1	-0.1	0.1
7	0.3	0.4	0.4	0.2	0.3
8	0.1	0.2	0.2	0.1	0.1
9	-0.6	-0.6	-0.5	-0.6	-0.6
10	0.1	0.2	0.3	0.3	0.3
11	0.0	0.0	0.0	0.0	0.0
12	-0.4	-0.4	-0.3	-0.4	-0.4
13	0.9	0.9	1.0	0.8	0.9
14	0.2	0.4	0.4	0.2	0.3
15	-0.9	-0.7	-0.6	-0.9	-0.6
16	-0.1	0.1	0.2	-0.1	0.2
Mean	**-0.1**	**0.0**	**0.1**	**0.0**	**0.1**

Table 16. Phase 2 Results: Standard Deviation of Difference between Measured and Modeled Results for the 767-400 Wallops Series 100 (difference in dB SEL for each POI)

POI	SC-Omni	SC-SOTR	DataSub-SOTR	DataSub-Dulles (Left)	DataSub-Dulles (Right)
6	0.1	0.2	0.2	0.4	0.4
7	0.3	0.3	0.3	0.3	0.3
8	0.3	0.3	0.3	0.4	0.3
9	0.3	0.2	0.2	0.3	0.2
10	0.3	0.4	0.4	0.3	0.4
11	0.0	0.0	0.0	0.0	0.0
12	0.3	0.2	0.2	0.2	0.2
13	0.3	0.3	0.3	0.4	0.3
14	0.3	0.2	0.2	0.5	0.3
15	0.2	0.2	0.2	0.5	0.4
16	0.1	0.2	0.2	0.5	0.4
Mean stdev	**0.2**	**0.2**	**0.2**	**0.3**	**0.3**

Polar Source Analysis

Table 17. Phase 2 Results: Average Difference between Measured and Modeled Results for the 767-400 Wallops Series 300 (difference in dB SEL for each POI)

POI	SC-Omni	SC-SOTR	DataSub-SOTR	DataSub-Dulles (Left)	DataSub-Dulles (Right)
6	0.5	0.7	0.7	0.5	0.5
7	0.7	0.8	0.8	0.7	0.7
8	0.6	0.7	0.7	0.6	0.6
9	-0.4	-0.4	-0.4	-0.5	-0.5
10	-0.5	-0.3	-0.4	-0.4	-0.4
11	0.0	0.0	0.0	0.0	0.0
12	-0.3	-0.2	-0.3	-0.3	-0.3
13	1.3	1.3	1.3	1.2	1.2
14	0.6	0.7	0.6	0.5	0.5
15	-0.5	-0.3	-0.4	-0.6	-0.6
16	0.7	0.8	0.8	1.1	1.0
Mean	**0.2**	**0.3**	**0.3**	**0.3**	**0.3**

Table 18. Phase 2 Results: Standard Deviation of Difference between Measured and Modeled Results for the 767-400 Wallops Series 300 (difference in dB SEL for each POI)

POI	SC-Omni	SC-SOTR	DataSub-SOTR	DataSub-Dulles (Left)	DataSub-Dulles (Right)
6	0.4	0.7	0.7	0.4	0.7
7	0.6	0.7	0.7	0.6	0.7
8	0.3	0.3	0.3	0.3	0.3
9	0.5	0.5	0.5	0.5	0.5
10	0.2	0.2	0.2	0.2	0.1
11	0.0	0.0	0.0	0.0	0.0
12	0.7	0.6	0.6	0.6	0.7
13	0.5	0.5	0.5	0.5	0.6
14	0.6	0.5	0.6	0.6	0.6
15	0.6	0.7	0.8	0.7	0.8
16	0.8	0.9	1.0	1.0	1.5
Mean stdev	**0.5**	**0.5**	**0.5**	**0.5**	**0.6**

When averaged across all events, most polar sources yielded similar results for all three scenarios (DC9-4 Wallops Series 100, 767-400 Wallops Series 100 and Series 300).

Since comparison of measurement and modeled data did identify a preferred polar source, the results were also evaluated as event averages across all the microphone positions (see Table 19 through Table 24).

Table 19. Phase 2 Results: Average Difference between Measured and Modeled Results for the DC9-4 Wallops Series 100 (difference in dB SEL for each Event)

Event	SC-Omni	SC-SOTR	DataSub-SOTR	DataSub-EMPA	DataSub-Dulles (Left)	DataSub-Dulles (Right)
110	-0.1	0.1	0.1	-0.9	0.0	0.2
121	0.2	0.2	0.2	0.3	0.3	0.3
130	0.1	0.2	0.1	0.1	0.1	0.2
140	0.2	0.4	0.4	1.2	0.6	1.1
150	0.3	-0.2	-0.3	-0.3	-0.4	-1.1
Mean	0.1	0.1	0.1	0.1	0.1	0.1
Stdev of Mean	0.12	0.20	0.21	0.69	0.33	0.68

Table 20. Phase 2 Results: Standard Deviation of Difference between Measured and Modeled Results for the DC9-4 Wallops Series 100 (difference in dB SEL for each Event)

Event	SC-Omni	SC-SOTR	DataSub-SOTR	DataSub-EMPA	DataSub-Dulles (Left)	DataSub-Dulles (Right)
110	0.61	0.67	0.64	0.62	0.64	0.67
121	0.51	0.53	0.50	0.52	0.52	0.49
130	0.54	0.54	0.54	0.48	0.52	0.57
140	0.42	0.51	0.46	0.82	0.57	0.74
150	0.39	0.31	0.31	0.33	0.31	0.46
Mean of Stdev	0.50	0.51	0.49	0.55	0.51	0.58
Max Stdev	0.61	0.67	0.64	0.82	0.64	0.74

Table 21. Phase 2 Results: Average Difference between Measured and Modeled Results for the 767-400 Wallops Series 100 (difference in dB SEL for each Event)

Event	SC-Omni	SC-SOTR	DataSub-SOTR	DataSub-Dulles (Left)	DataSub-Dulles (Right)
110	-0.1	-0.1	0.0	0.1	-0.1
112	0.2	0.2	0.3	0.3	0.3
120	-0.2	-0.2	0.0	-0.2	-0.1
121	-0.1	0.0	0.0	0.1	-0.1
140	-0.2	0.2	0.3	0.0	0.3
150	-0.1	0.1	0.1	-0.4	0.0
160	0.0	0.1	0.1	0.1	0.1
Mean	-0.1	0.0	0.1	-0.1	0.0
Stdev of Mean	0.13	0.13	0.11	0.19	0.17

Table 22. Phase 2 Results: Standard Deviation of Difference between Measured and Modeled Results for the 767-400 Wallops Series 100 (difference in dB SEL for each Event)

Event	SC-Omni	SC-SOTR	DataSub-SOTR	DataSub-Dulles (Left)	DataSub-Dulles (Right)
110	0.44	0.44	0.44	0.42	0.44
112	0.49	0.45	0.46	0.47	0.47
120	0.52	0.52	0.50	0.52	0.52
121	0.51	0.50	0.47	0.48	0.49
140	0.56	0.61	0.60	0.56	0.59
150	0.50	0.48	0.46	0.75	0.50
160	0.60	0.60	0.59	0.60	0.59
Mean of Stdev	0.52	0.54	0.53	0.58	0.54
Max Stdev	0.60	0.61	0.60	0.75	0.59

Polar Source Analysis

Table 23. Phase 2 Results: Average Difference between Measured and Modeled Results for the 767-400 Wallops Series 300 (difference in dB SEL for each Event)

Event	SC-Omni	SC-SOTR	DataSub-SOTR	DataSub-Dulles (Left)	DataSub-Dulles (Right)
310	0.3	0.4	0.4	0.3	0.3
321	0.4	0.3	0.3	0.4	0.2
330	-0.4	-0.4	-0.5	-0.4	-0.6
340	0.6	0.9	1.0	1.0	1.3
350	0.1	0.5	0.5	-0.1	0.3
360	0.6	0.7	0.7	0.6	0.7
Mean	0.3	0.4	0.4	0.3	0.4
Stdev of Mean	0.35	0.43	0.47	0.44	0.57

Table 24. Phase 2 Results: Standard Deviation of Difference between Measured and Modeled Results for the 767-400 Wallops Series 300 (difference in dB SEL for each Event)

Event	SC-Omni	SC-SOTR	DataSub-SOTR	DataSub-Dulles (Left)	DataSub-Dulles (Right)
310	0.60	0.61	0.61	0.59	0.60
321	0.58	0.55	0.55	0.57	0.56
330	0.66	0.65	0.69	0.67	0.70
340	0.91	0.92	0.96	1.02	1.13
350	0.64	0.74	0.74	0.58	0.68
360	0.85	0.83	0.81	0.84	0.85
Mean of Stdev	0.71	0.72	0.73	0.71	0.75
Max Stdev	0.91	0.92	0.96	1.02	1.13

When considering the average difference between each polar source and the corresponding measurement data for each Phase 2 events (DC9-4 Wallops 100 series, 767-400 Wallops 100 series, and 767-400 Wallops 300 series), the polar source generated using the AEDT spectral class and the start-of-takeoff-roll directivity planned for AEDT 3 performed slightly better than the other polar sources, with data submittal spectra and the start-of-takeoff-roll directivity planned for AEDT 3 coming in as a close second. However, it should be noted that most polar sources yielded similar results for all three scenarios (DC9-4 Wallops Series 100, 767-400 Wallops Series 100 and Series 300).

4.3 Contour Comparison

The Phase 1 and Phase 2 analyses showed some differences between the different types of polar sources at a range of locations near a flight path, but they do not capture the impact of fore and aft directivity on the noise levels at the receptors. In order to get a better feel for the overall impact of the polar sources on the noise levels over a larger area (e.g., neighborhoods near an airport), a contour analysis was conducted. A short segment flight track was modeled in AAM with various different polar sources, in order to produce contour footprints that showcase the directivity associated with polar sources. The polar sources used for the contour analysis are listed in Table 25.

Table 25. Polar Sources Used in the Contour Analysis

	767-400 departure (full power takeoff flaps, accelerating - based on Wallops 100 series)		767-400 approach (low power with flaps, constant speed - based on Wallops 300 series)	
Directivity	**Spectral Class**	**Data Submittal**	**Spectral Class**	**Data Submittal**
Omni	Y		Y	
AEDT2 SOTR				
AEDT3 Jet SOTR	Y		Y	Y
EMPA				
Dulles - Left		Y	Y	
Dulles - Right		Y	Y	

The contour results from these runs are presented in Figure 13 through Figure 22.

Polar Source Analysis

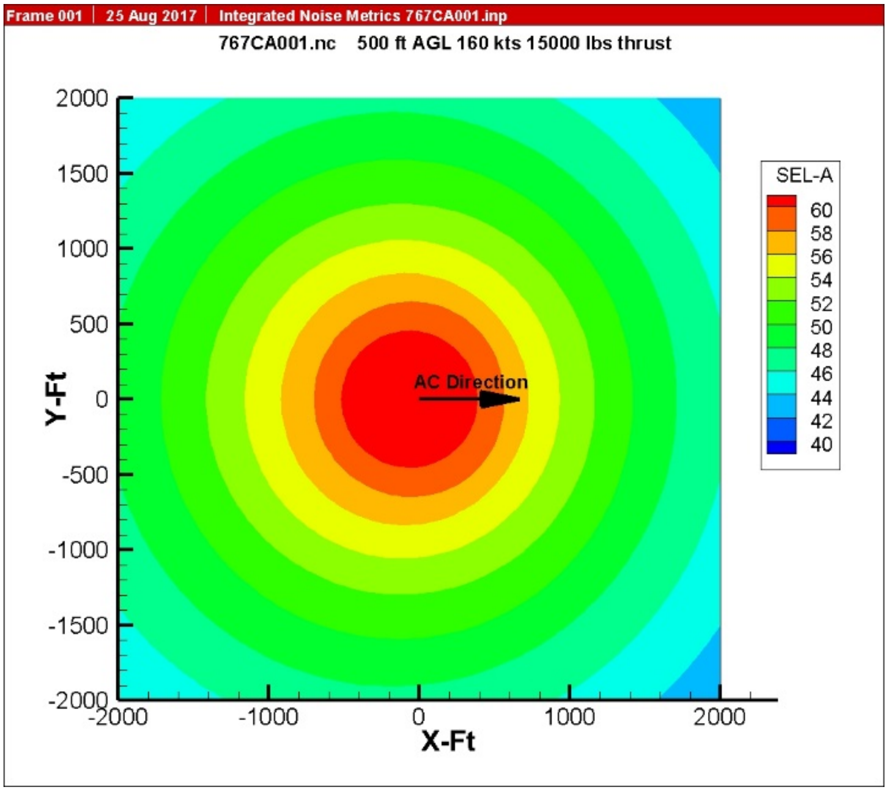

Figure 13. Contour for 767-400 Approach with Polar Source Using Spectral Class Data and Omnidirectional Directivity

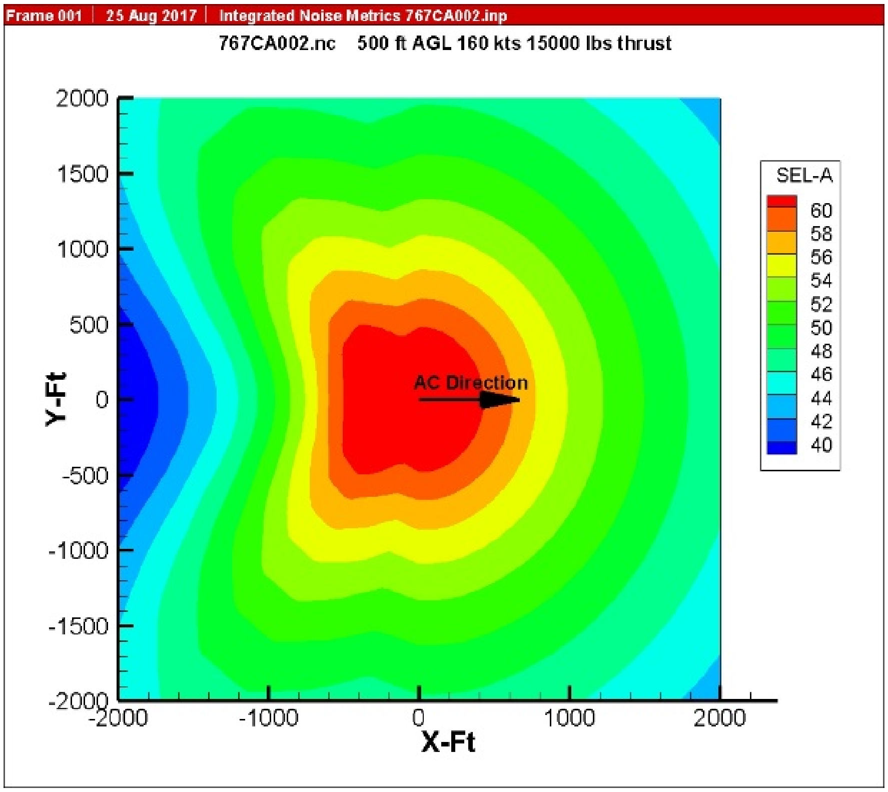

Figure 14. Contour for 767-400 Approach with Polar Source Using Spectral Class Data and SAE-AIR-6207 (AEDT 3) Directivity

Polar Source Analysis

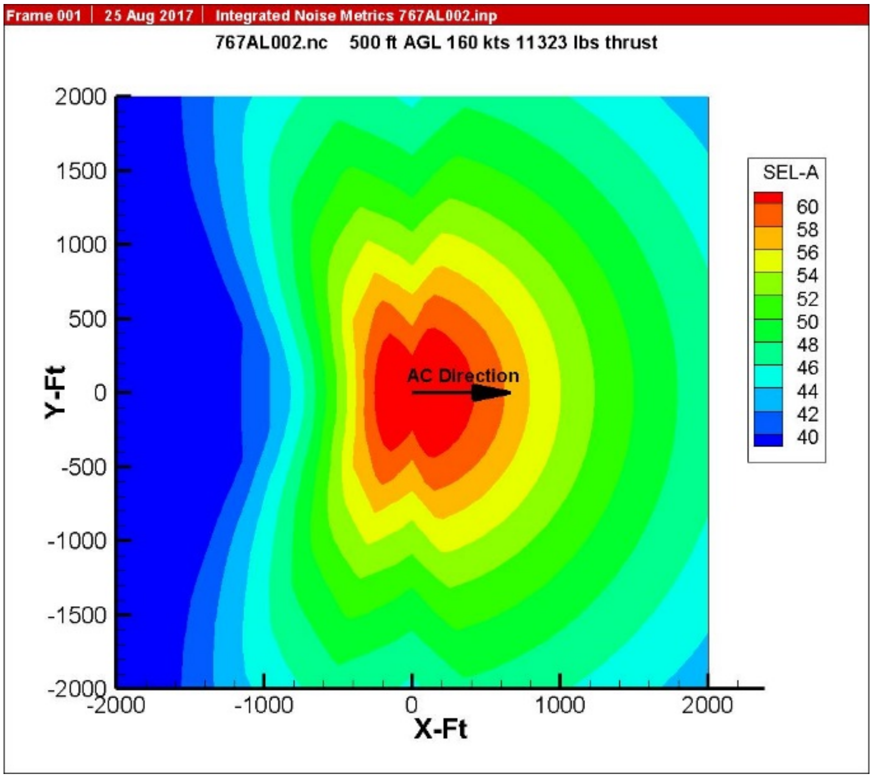

Figure 15. Contour for 767-400 Approach with Polar Source Using Spectral Class Data and Dulles Directivity (Left)

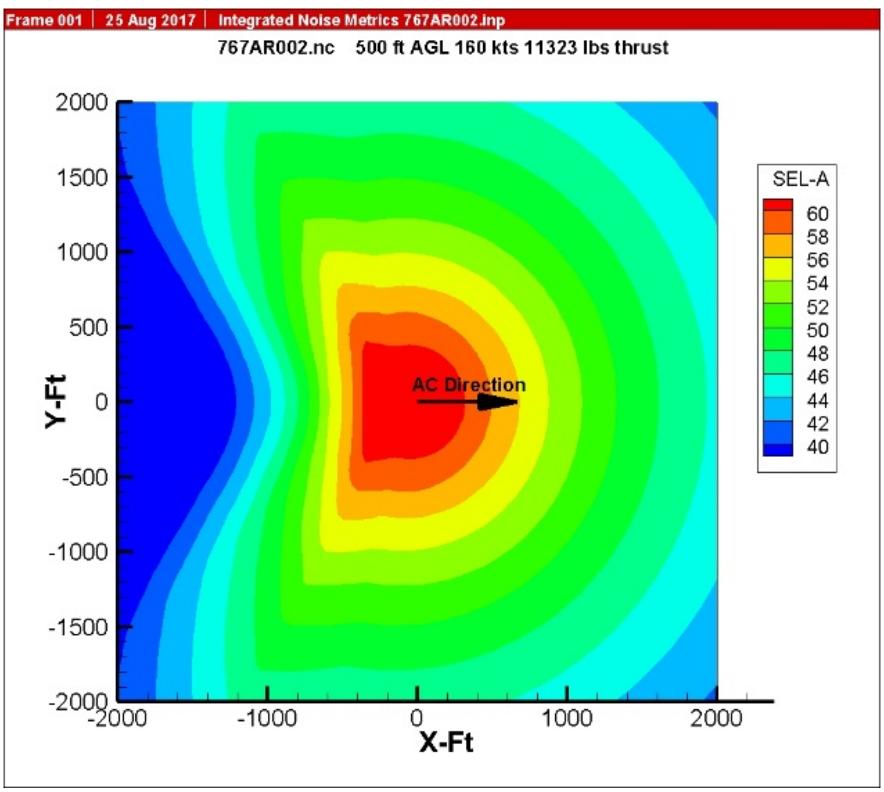

Figure 16. Contour for 767-400 Approach with Polar Source Using Spectral Class Data and Dulles Directivity (Right)

Polar Source Analysis

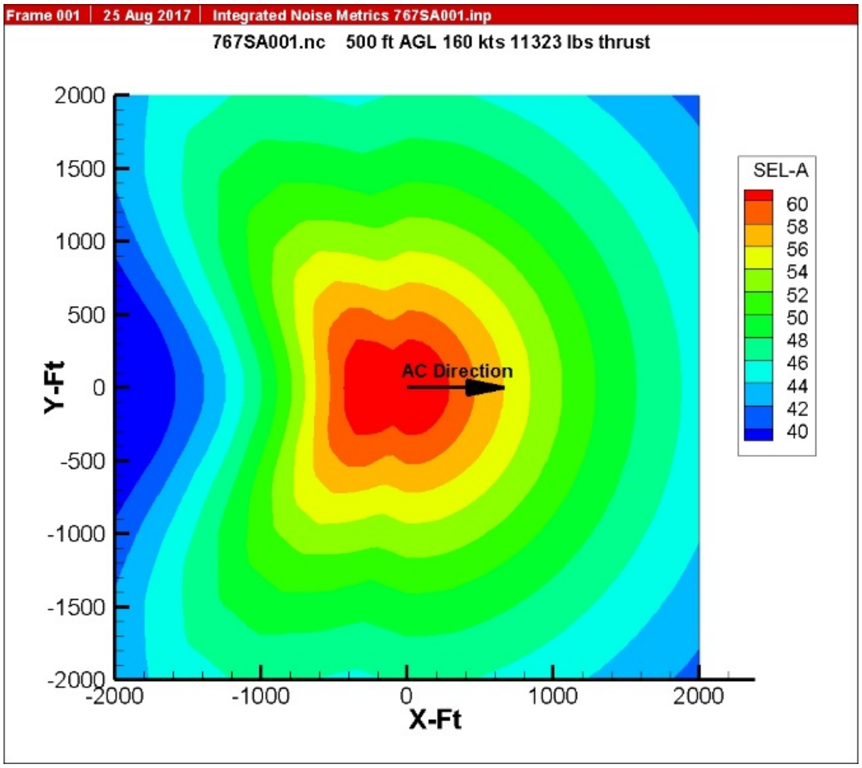

Figure 17. Contour for 767-400 Approach with Polar Source Using Submitted Spectral Data and SAE-AIR-6297 (AEDT 3) Directivity

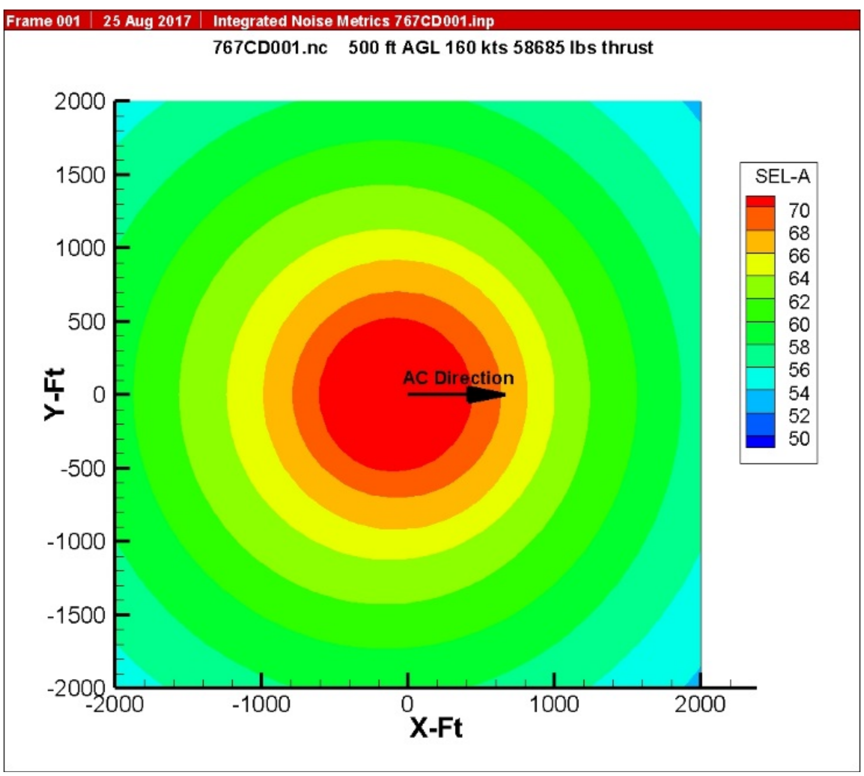

Figure 18. Contour for 767-400 Departure with Polar Source Using Spectral Class Data and Omnidirectional Directivity

Polar Source Analysis

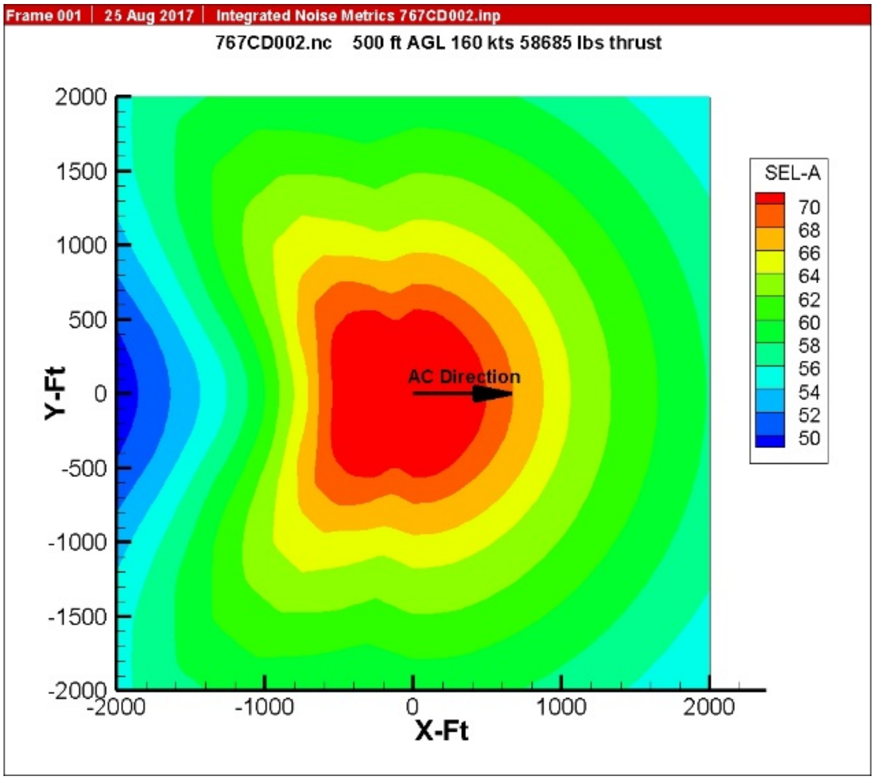

Figure 19. Contour for 767-400 Departure with Polar Source Using Spectral Class Data and SAE-AIR-6297 (AEDT 3) Directivity

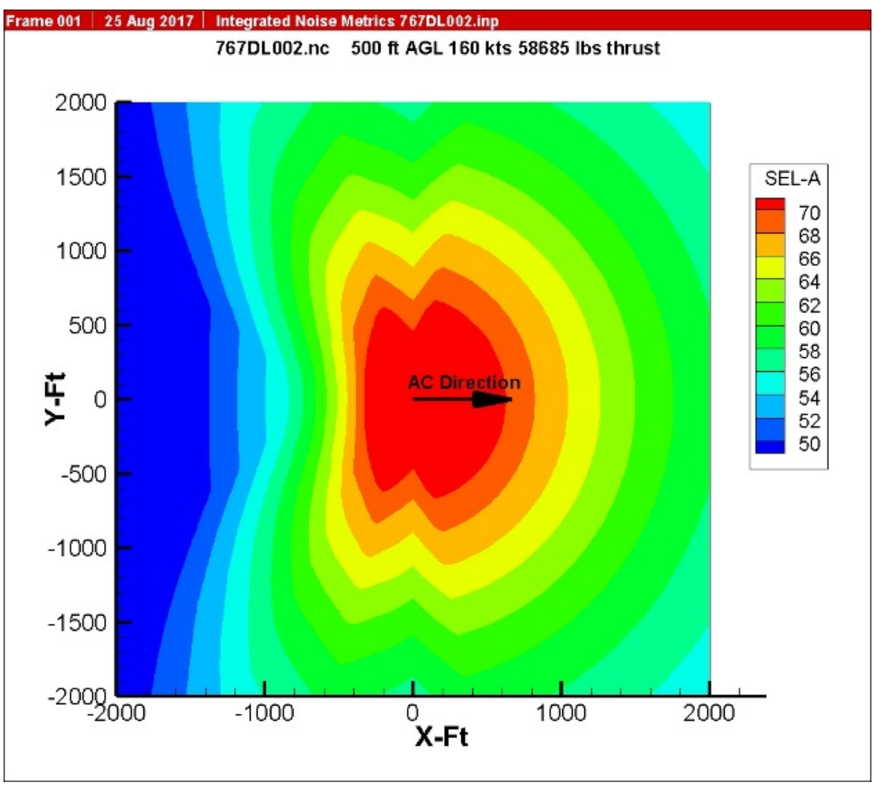

Figure 20. Contour for 767-400 Departure with Polar Source Using Submitted Spectral Data and Dulles Directivity (Left)

Polar Source Analysis

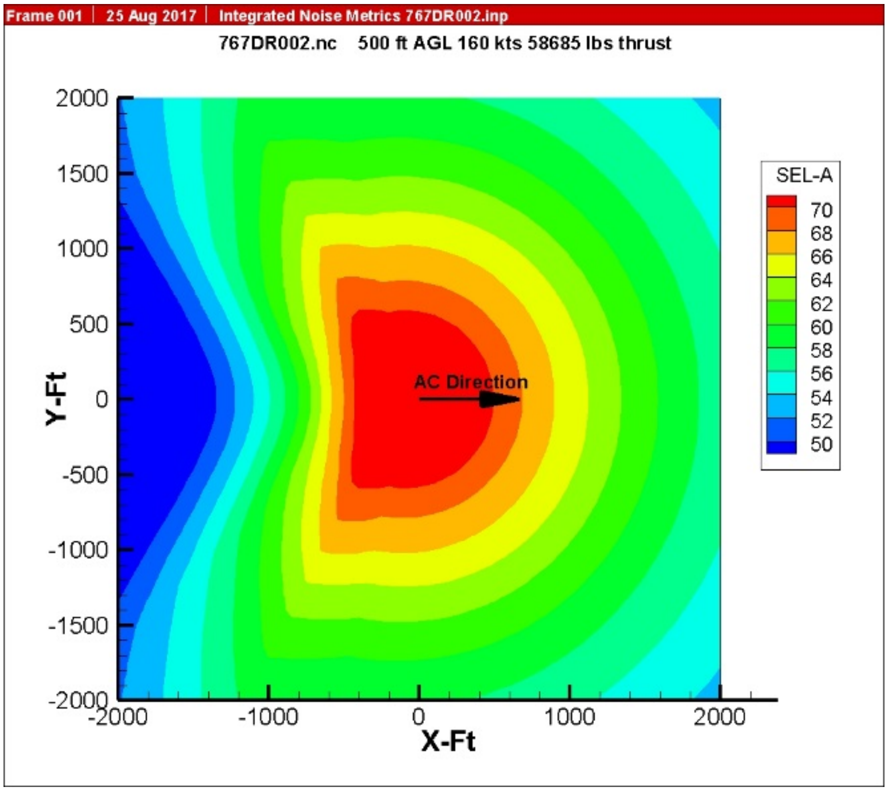

Figure 21. Contour for 767-400 Departure with Polar Source Using Submitted Spectral Data and Dulles Directivity (Right)

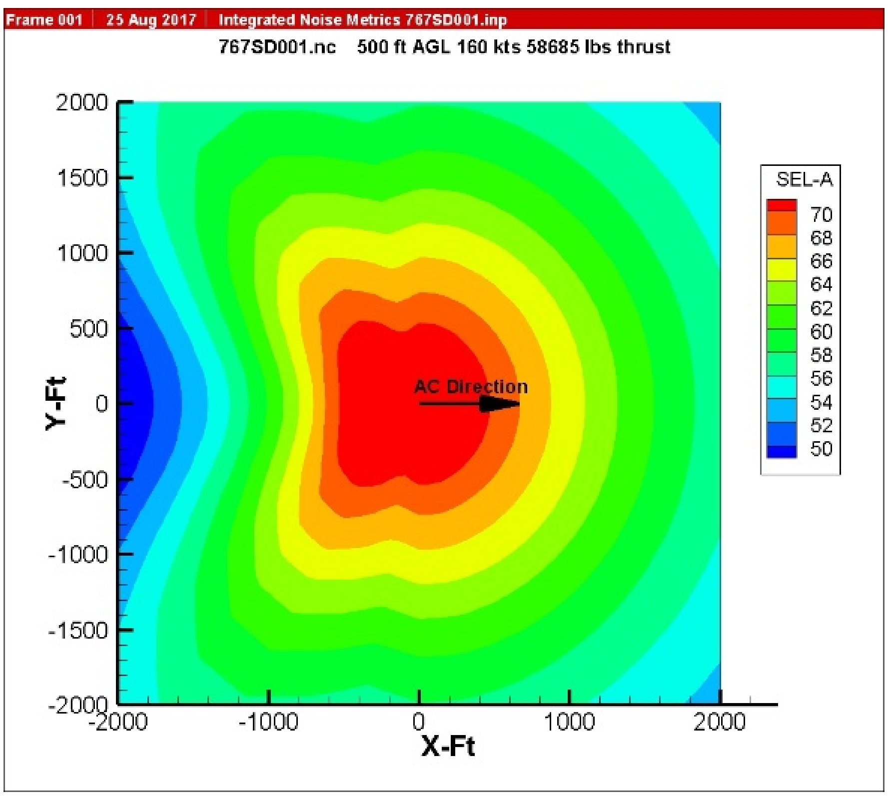

Figure 22. Contour for 767-400 Departure with Polar Source Using Submitted Spectral Data and SAE-AIR-6297 (AEDT 3) Directivity

The contouring exercise shows that polar source directivity can have a direct and significant impact on the shape of noise contours

5 Implementation in AEDT and Other FAA Tools

The current version of AEDT includes an NPD and spectral class database that couple noise propagation and noise sources with limited directivity and spectral variation options. Polar sources are significantly different from the current AEDT data sources, and they will require updates to AEDT code and algorithms, in order to support their implementation as a new AEDT data format. In order for AEDT to utilize polar sources, the following updates would need to be made to AEDT and the AEDT FLEET database:

1. A separate noise propagation method would need to be implement in AEDT that is not integrated with the noise database;
2. A polar source database would need to be developed for all aircraft in AEDT leverage existing data wherever possible and utilizing the methods recommended in this paper, and that database would need to be structured with enough flexibility that would allow for High Fidelity polar sources to be integrated into the database, once they are developed;
3. Develop guidance for developing High Fidelity polar source data;
4. Directivity based adjustments that are used in polar source development (start-of-takeoff-roll directivity and lateral attenuation) will need to be removed from the AEDT noise computations, to avoid double counting;
5. Frequency-based adjustments in AEDT will need to be modified to accept polar source spectral data (most of which will just be code restructuring and bookkeeping); and
6. AEDT noise computation methods will need to be developed to accommodate polar source spectral data, including a method to interpolate/extrapolate spectral data, when necessary.
7. Advanced flight path segmentation techniques would need to be implemented, such as those discussed in recent FAA-funded research[29,41], in order to take full advance of the polar source directivity.

Although AEDT is not currently structured to utilize polar sources, FAA’s Ray Model does accept source data similar to polar sources[27,39]. It could also be utilized by a ray-based ground impedance model, such as those recommended in ACRP 02-52 “Improving AEDT Noise Modeling of Hard, Soft, and Mixed Ground Surfaces[42]”. It could also be used to independently improve some of the existing frequency-based noise adjustments in AEDT. In addition, polar sources coupled with advanced flight path segmentation and scheduling could be used to investigate the feasibility of implementing simulation modeling in AEDT.

6 Conclusions and Recommendations

The goals for this effort were to:

1. Identify a method for developing polar acoustic sources for aircraft, to be utilized for future aircraft model development,
2. Identify existing measurement data which could be leveraged in the creation of polar noise sources
3. Develop sample 3-D polar source data sets for several different aircraft, and

4. Develop recommendations for implementing the 3-D polar source method in AEDT, including changes to the AEDT database.

This analysis identified a method for combining calibrated spectral data with directivity data to generate polar sources. It allowed for Basic Fidelity polar sources to be developed with AEDT data alone (spectral classes, NPDs, and directivity adjustments), while allowing for Medium and High Fidelity sources to be developed using similar methods, when higher fidelity source data are available. Some of those higher fidelity data sources could be AEDT ANP data submittals, manufacturer data, measurement data and external databases (like EMPA's FLULA2 data set), if they are publically available.

As a proof of concept, Basic and Medium Fidelity sources were developed leveraging AEDT and other data sources for this analysis and were run through an external noise modeling tool (AAM). This analysis showed that polar sources could be used to run single aircraft events to generate noise results, indicating that they are functionally equivalent when looking at integrated model results like SEL and LAMAX. However when ready, more advanced directivity can be put into AEDT through the use of polar sources, as a part of incremental improvements to the tool.

7 Potential Future Work

This effort was a preliminary analysis to show a proof of concept that polar sources could be developed from existing data and could be utilized to yield aircraft noise results similar to AEDT. Potential future work could include the following:

1. Leveraging existing data to expand the polar source data set;
2. Expand the polar source investigation to include aircraft data with more complex spectral directivity issues, such as deployed landing gear and flaps (possibly utilizing ANOPP sources being developed for ASCENT projects);
3. Expand the noise analysis to include expanded contour and spectral time history analyses;
4. Expand the modeling effort to include more complex operations, such as turns;
5. Expand the modeling effort to include full airport analyses;
6. Develop guidance for developing polar sources of various fidelity;
7. Finalize noise propagation methods in AEDT that utilize polar sources, and
8. Assisting the AEDT development team in scoping improvements to AEDT that would allow for the inclusion of polar sources in the model.

8 References

1. Meghan Ahearn, et al., Aviation Environmental Design Tool (AEDT) Version 2c Service Pack 2 Technical Manual, U.S. Department of Transportation John A. Volpe National Transportation Systems Center, DOT-VNTSC-FAA-17-08, (March 2017).

2. FAA ASCENT, Project 43, Noise Power Distance Re-Evaluation, https://ascent.aero/project/noise-power-distance-re-evaluation/ , September 6, 2017.

3. SAE International, Committee A-21, Aircraft Noise, Procedure for the Calculation of Airplane Noise in the Vicinity of Airports, Aerospace Research Report No. 1845, Warrendale, PA: SAE International, September 1995.

4. SAE International, Committee A-21, Aircraft Noise, Method for Predicting Lateral Attenuation of Airplane Noise, Aerospace Information Report No. 5662, Warrendale, PA: SAE International, April 2006.

5. Farassat, F. and Jay H. Casper, “Towards an Airframe Nosie Prediction Methodology: Survey of Current Approaches” AIAA-2006-0210, 2006.

6. Thomas, R. et al., “Hybrid Wing Body Aircraft System Noise Assessment with Propulsion Airframe Aeroacoustic Experiments”, AIAA 2010-3913, 2010.

7. Burley, C. et al., “ANOPP Landing Gear Noise Prediction Comparisons to Model-Scale Data”, AIAA 2007-3459, May 2007.

8. Guo, Y., “Empirical Prediction of Aircraft Landing Gear Noise,” NASA Contractor Report 2005-213780, July 2005.

9. Guo, Y., “A Semi-Empirical Model for Aircraft Landing Gear Noise Prediction,” AIAA Paper 2006-2627, 12th AIAA/CEAS Aeroacoustics Conference, Cambridge, Massachusetts, May 2006.

10. Horne, W.C., et al., “Aeroacoustic Study of a 26%-Scale Semispan Model of a Boeing 777 Wing in the NASA Ames 40- by 80-Foot Wind Tunnel,” NASA Technical Paper 2004-212802, October 2004.

11. Stoker, R., and Sen, R., “An Experimental Investigation of Airframe Noise Using a Model-Scale Boeing 777,” AIAA Paper 2001-0987, 39th AIAA Aerospace Sciences Meeting, Reno, NV, 2001.

12. Humphreys, W., and Brooks, T., “Noise Spectra and Directivity For a Scale-Model Landing Gear,” AIAA Paper 2007-3458, 13th AIAA/CEAS Aeroacoustics Conference, Rome, Italy, May 21-23, 2007.

13. Mehdi R. Khorrami and Ehab Fares. "Simulation-Based Airframe Noise Prediction of a Full-Scale, Full Aircraft", 22nd AIAA/CEAS Aeroacoustics Conference, Aeroacoustics Conferences, (AIAA 2016-2706), 2016.

14. SAE International, Committee A-21, Aircraft Noise, Modeling Line-of-Sight Blockage of Aircraft Noise, Aerospace Information Report No. 6297, Warrendale, PA: SAE International, 2017.

15. Schultz, Troy et al., "Development of a Noise Source Database for an Aircraft Simulation Model", Noise-Con 2011, Portland Oregon, July 2011.

16. Schultz, Troy et al., "Preparation of AAM Noise Spheres for Legacy NOISEFILE Aircraft" Defense Noise Working Group Publication, Wyle Research Report No. TN 12-17, October 2012.

17. Ikelheimer, Bruce, Noise Model Simulation (NMSim) User's Manual, Wyle Research Report No. WR 03-09, June 2005.

18. Welker, Kurt, "IMOM Acoustic Modeling", Joint Tactical Aeroacoustics Conference, January 2007.

19. Zorumski, W.E, Aircraft Noise Prediction Program Theoretical Manual, NASA TM-83199 Part 2, February 1982.

20. NASA, "Spring 2016 Acoustics Technical Working Group Meeting", April 19-20, Hampton Va., 2016.

21. Environmental Design Space (EDS), https://www.faa.gov/about/office_org/headquarters_offices/apl/research/models/eds/

22. Lytle, J. K., The Numerical Propulsion System Simulation: An Overview, NASA TM 209915, National Aeronautics and Space Administration, 2000.

23. Page, Juliet, "Turbofan and Propeller Aircraft Taxi Operating State Noise Power Distance and Spectral Class Database Development Process for AEDT", SciTech, AIAA-2014-0366, January 2014.

24. Page, Juliet, et al., "Enhance Modeling of Aircraft Taxiway Noise, Volume 2. Aircraft Taxi Noise Database and Development Process", ACRP 02-27 Web-Only Document 9, January 2013.

25. Mavris, Dimitri, et al., "Noise Power Distance Re-evaluation, Project 43", ASCENT 43 review meeting, July 2017.

26. Fleming, Gregg, et al., Engine Installation Effects of Four Civil Transport Airplanes: Wallops Flight Facility Study, NASA/TM-2003-212433, October 2003.

27. Page, J. et al., "Advanced Acoustic Model Technical Reference and User Manual," Department of Defense Strategic Environmental Research and Development Program (SERDP) Project WP-1304, and Wyle Research Report WR 08-12, May 2009. http://www.serdp-estcp.org/content/download/9133/109364/file/WP-1304-TR.pdf.

28. SAE International, Committee A-21, Aircraft Noise, Prediction Method for Lateral Attenuation of Airplane Noise During Takeoff and Landing, Aerospace Information Report No. 1751, Warrendale, PA: SAE International, March 1981.

29. Page, Juliet, Acoustics Modeling in AEDT: Long Term Vision and Development Roadmap, September 2016 (draft).

30. James, Michael et al., NoiseMap and AEDT Gap Analysis, US DOT / Volpe Report publication pending, submitted September 2017.

31. Bradley, Kevin et al., Advanced Acoustic Model Technical Reference and User Manual, Wyle Research Report WR 16-08, July 2017.

32. Pietrzko and Bütikofer, FLULA – Swiss Aircraft Noise Prediction Program, Annual Conference of the Australian Acoustical Society, 2002.

33. Krebs, Bütikofer, Plüss and Thomann, Sound Source Data for Aircraft Noise Simulation, ACTA ACUSTICA, 2004.

34. Lau, Michael et al., Behind Start of Take-off Roll Aircraft Sound Level Directivity Study - Revision 1, DOT-VNTSC-NASA-12-01, NASA/TM-2012-217783, April 2015.

35. Rew, R., "NetCDF User's Guide, An Interface for Data Access Version 2.3," April 1993. Available from: ftp.unidata.ucar.edu.

36. Hobbs, Chris et al., "Acoustic Repropagation Technique and Practical Source Characterization for Simulation Noise Model Databases", Noise-Con 2010, Baltimore, MD, 2010.

37. Krebs, W., and G. Thomann, "Lateral Directivity of Aircraft Noise", Acou. Soc. Am, EuroNoise/Acoustics '08, Paris, 2008.

38. Veltin, Jeremy et al., "Improvement of Community Noise Models for Aircraft Noise Prediction", AIAA Aerospace Sciences Meeting, AIAA-2008-12, Reno NV, January 2008.

39. Page, Juliet, "AEDT-Ray SEL Implementation Plan", Technical Memorandum, July 2015.

40. Boeker, Eric and Page, Juliet, "AEDT-Ray Model: Code Structure Options", Technical Presentation to FAA AEE, April 26, 2016.

41. Plotkin, Kenneth J., et al., Detailed Weather and Terrain Analysis for Aircraft Noise Modeling, DOT-VNTSC-FAA-14-08, Wyle Report 13-01, April 2013.

42. Hobbs, Chris, et al., “Improving AEDT Noise Modeling of Mixed Ground Surfaces”, ACRP 02-52 Web-Only Document 32, June 2017.

9 Appendices

9.1 Spherebuilder Description

In use, the tool reads the keywords and associated data, and executes the commands in sequence. Note that running the code using a different keyword sequence may result in different polar source results.

Table 26. SphereBuilder Keywords

Keyword	Description
ADDALL	Value in dB to be added to all frequencies/directions
DIRECT-A	Filename w/ delta-dBA theta direct. (#pts|Ang,del-dBA)
DOPPLER	Doppler Effect (freq shift) is added for specified speed
EXTRACT	Single (Phi, Theta) spectra to extract from DATfile to SPECIAL
LATDIR	Applies AEDT engine installation effects (WING or FUSELAGE)
PASTEALL	Put SPECIAL spectra everywhere
RCONVERT	New Radius. Conversion based on Spherical Spreading
SOTR	Start of Takeoff Roll SLRseg smoothing function from AEDT

ADDALL: This keyword adds the user specified value (in dB) to all one-third octave bands in all directions. Generally this is used towards the end to 'calibrate' the sphere to provide a known level at a specific point. For example ADDALL is used as the last step to ensure the polar source yields the specified NPD integrated SEL value for steady level flight at 160 knots at the specified NPD Distance height above a centerline 4ft Receiver over uniform soft ground.

DIRECT-A: Angular directivity is specified by the user in an external file (see Table 27) in columnar format (angle, dB) where 0^{o} is the nose and 180^{o} is the tail of the vehicle. This is linearly interpolated and applied to each one-third octave band for all roll angles in the spheres at the specified fore-aft angle. This keyword can be used with empirical data, with averaged directivity patterns (such as are applied in AEDT behind the start of takeoff roll) or by using other analytical directivity shapes as one could develop using ANOPP or first principles modeling.

Table 27. Angular directivity examples (A-320 and DC-9) for the DIRECT-A keyword

A-320	
0	0
15	-0.493997918
30	-0.950363613
45	-0.941740544
60	-1.588547438
75	-2.141309284
90	-1.366982733
105	-1.045014626
120	-2.804939969
135	-5.570349491
150	-9.070383724
165	-13.51402226
180	-15.8504333

DC-9	
0	0
15	0.084307941
30	0.68990598
45	1.467851943
60	1.862312087
75	3.347957418
90	6.533283453
105	9.277318428
120	11.14188647
135	12.79351097
150	10.93546962
165	4.133687024
180	-0.11644777

DOPPLER: This keyword applies Doppler frequency shift to the spectrum for each point on the polar source based on the speed of the vehicle and its direction (Euler angle). The Doppler multiplier (Equation 1) provides new lower and upper frequency limits. The tool assumes the un-shifted acoustic energy is uniformly spread across the original standard one-third octave bands. After computing the new upper and lower frequencies it apportions the energy back into the standard one-third original bands. The Doppler multiplier may be expressed as

$$f' = f\left[\frac{1}{1+\frac{u}{c}}\right] \qquad \text{Equation 1}$$

Where f' is the Doppler shifted frequency, based on the stationary frequency, f with u/c representing the component of the aircraft speed (u) in the direction of the receiver divided by the local speed of sound, c. In this project the AEDT spectral class data was generally applied to a polar source in all directions, then Doppler shifted using Equation 1, resulting in different spectrum presenting in different directions. Note that this process can lose some energy due to binning and shifting above the top band or below the bottom band. No attempts were made to mitigate that as it was determined that slight changes in these bands would not greatly affect the EPNL or dBA based noise metric calculations.

EXTRACT. This is a simple way to extract a single line of spectral data from an ASCII .DAT formatted file. It allows the user to specify a starting spectrum, such as one from the AEDT spectral class data, or from empirical data. It stores it for use later, typically with the PASTEALL keyword.

LATDIR. Lateral Directivity based on the source directivity due to engine installation effects as prescribed in AEDT is applied to the polar source when this keyword is used. The user specifies if the aircraft has the engines mounted on the wings or on the fuselage and the tool applies the lateral directivity relationship described in Section 2.2.1.

PASTEALL. This keyword takes the spectrum previously stored in memory by the EXTRACT keyword and applies it to all directions on the polar source. It is typically used in conjunction with the EXTRACT keyword.

RCONVERT. This converts, using only spherical spreading, the acoustic energy in the polar source prescribed at one radius to a different radius. The process is based on the AAM compact source convention where the radius only affects spherical spreading and all other acoustic energy (absorption and propagation effects) are applied from the sphere center.

SOTR. This keyword applies the AEDT ground based start of takeoff roll directivity at azimuthal angles to the polar source. This is the same start-of-takeoff-roll directivity defined in SAE-AIR-1845[3] and included in AEDT 2c SP2[1]. The dB adjustment is applied to all one-third octave bands at the prescribed angles, defined from 90º (abeam) to 180º (aft) based on Equations 4-54 and 4-55 of the AEDT 2c SP2 Technical Manual[1] and is represented in Figure 23. A user specified distance may also be considered, since AEDT dilutes the effect of the directivity for distances greater than 2500 ft as described in Equation 4-56 of the AEDT 2c SP2 Technical Manual[1].

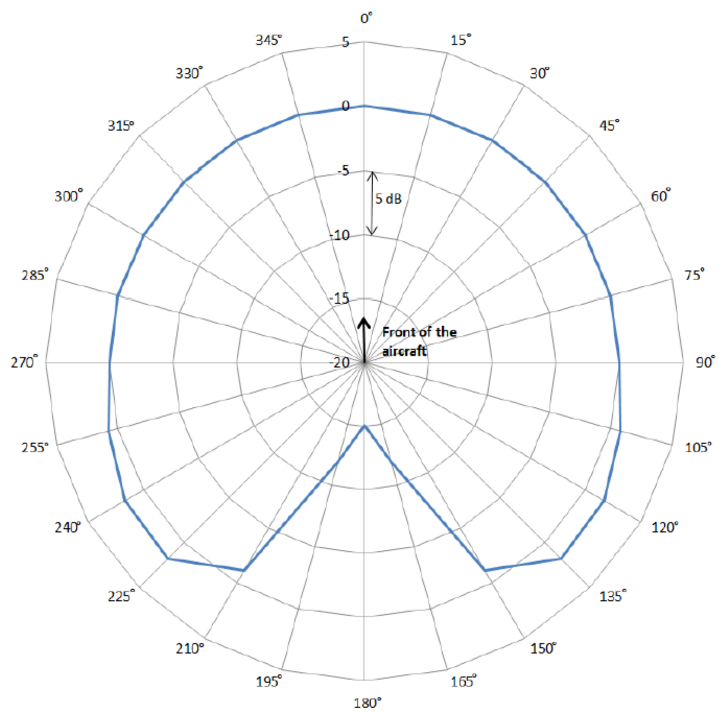

Figure 23. Ground based directivity adjustment applied in AEDT.

9.2 Appendix: Phase 1 Results

This appendix includes the Phase 1 noise difference results for each event.

Table 28. Phase 1 DC9-4 LAMAX Difference Results (Wallops – Modeled) by Event for the Wallops 400 Series

		Difference (Wallops Data - Modeled Results)							
Event	POI	AEDTSC_omni	AEDTSC_AEDT2	AEDTSC_AEDT3	AEDTSC_EMPA	Data_AEDT2	Data_AEDT3	Data_EMPA	Data_Dulles (Left)
410	P06	-1.5	-0.9	-1.5	-2.4	-1.4	-1.9	-3.4	-2.0
410	P07	-1.9	-1.4	-2.1	-3.1	-1.9	-2.7	-4.0	-2.6
410	P08	-1.6	-1.1	-1.9	-2.9	-1.7	-2.5	-3.6	-2.3
410	P09	-0.4	0.0	-0.8	-1.9	-0.6	-1.4	-2.4	-1.2
410	P10	-1.2	-0.9	-1.7	-2.5	-1.3	-2.1	-2.9	-1.8
410	P11	-0.7	-0.4	-1.2	-2.3	-1.0	-1.8	-2.8	-1.6
410	P12	-0.3	0.1	-0.7	-1.8	-0.5	-1.3	-2.4	-1.1
410	P13	-1.9	-1.5	-2.2	-3.3	-1.9	-2.7	-4.0	-2.7
410	P14	-1.0	-0.6	-1.2	-2.2	-1.0	-1.7	-3.0	-1.7
410	P15	-0.7	-0.1	-0.6	-1.5	-0.5	-1.0	-2.6	-1.2
420	P06	0.7	0.5	0.8	-0.3	0.1	0.3	-1.3	0.9
420	P07	-1.3	-1.9	-1.7	-2.9	-2.4	-2.2	-3.6	-2.0
420	P08	-0.8	-1.5	-1.3	-2.5	-2.0	-1.9	-3.3	-1.9
420	P09	-0.3	-1.1	-1.0	-2.2	-1.6	-1.5	-2.8	-1.6
420	P10	-1.8	-2.7	-2.5	-3.8	-3.1	-3.0	-4.2	-3.1
420	P11	0.7	-0.3	-0.2	-1.5	-0.9	-0.8	-2.0	-1.1
420	P12	2.1	1.1	1.2	0.0	0.6	0.7	-0.5	0.5
420	P13	1.2	0.4	0.4	-0.8	-0.1	0.0	-1.3	-0.2
420	P14	0.7	-0.1	0.1	-1.1	-0.6	-0.4	-1.8	-0.4
420	P15	1.2	1.0	1.1	0.1	0.5	0.6	-0.9	1.0
440	P06	-1.3	0.2	0.5	0.7	-0.3	-0.1	-1.5	1.1
440	P07	-0.3	0.7	1.2	0.9	0.0	0.5	-0.9	1.6
440	P08	0.1	0.5	1.0	0.5	-0.2	0.3	-1.0	1.5
440	P09	1.0	1.0	1.5	0.8	0.2	0.7	-0.4	2.0
440	P10	-1.8	-2.2	-1.7	-2.5	-2.8	-2.3	-3.1	-1.0
440	P11	0.3	-0.2	0.3	-0.6	-1.0	-0.6	-1.5	0.8
440	P12	1.4	1.3	1.8	1.1	0.6	1.0	0.0	2.4
440	P13	-0.3	0.1	0.5	0.0	-0.7	-0.2	-1.4	1.1
440	P14	-0.1	0.8	1.3	0.9	0.1	0.6	-0.9	1.7
440	P15	0.3	1.8	2.0	2.2	1.2	1.5	0.1	2.7

Table 25. Phase 1 DC9-4 LAMAX Difference Results (Wallops – Modeled) by Event for the Wallops 400 Series (cont.)

		Difference (Wallops Data - Modeled Results)							
Event	POI	AEDTSC_omni	AEDTSC_AEDT2	AEDTSC_AEDT3	AEDTSC_EMPA	Data_AEDT2	Data_AEDT3	Data_EMPA	Data_Dulles (Left)
450	P06	-0.4	0.2	0.2	-1.0	-0.3	-0.3	-3.3	-0.7
450	P07	0.3	0.4	0.7	-1.4	-0.2	0.1	-3.2	-1.0
450	P08	1.1	0.8	1.4	-1.5	0.1	0.8	-3.0	-0.8
450	P09	3.1	2.4	3.1	-0.4	1.8	2.4	-1.6	0.6
450	P10	2.4	1.5	1.9	-1.3	1.0	1.4	-1.8	-0.2
450	P11	4.1	3.5	3.6	0.9	2.8	2.9	0.1	1.6
450	P12	3.9	3.3	3.7	0.6	2.7	3.0	-0.4	1.4
450	P13	1.8	1.3	1.9	-1.5	0.6	1.2	-2.7	-0.5
450	P14	1.5	1.2	1.7	-0.9	0.6	1.1	-2.4	-0.2
450	P15	0.3	0.5	0.6	-0.9	0.0	0.0	-2.9	-0.6

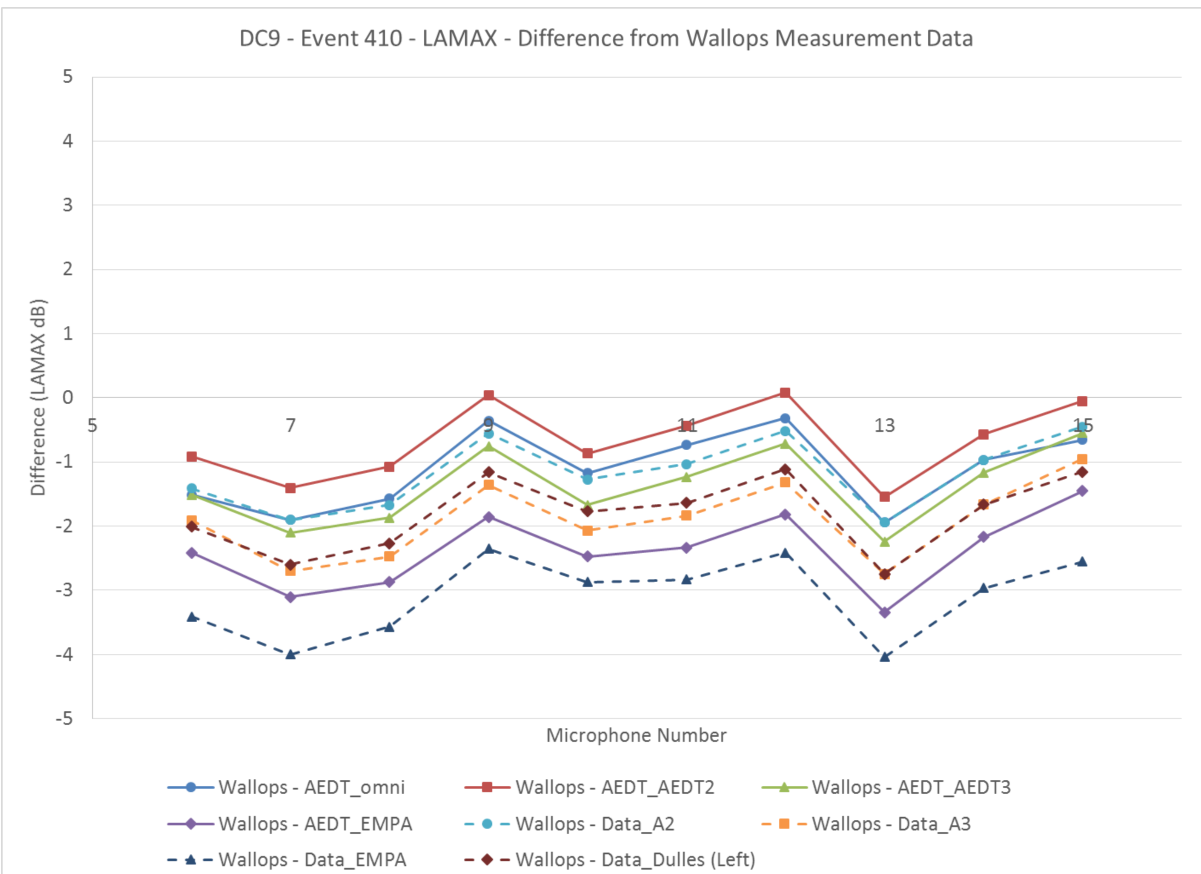

Figure 24. Phase 1 DC9-4 LAMAX Difference Results (Wallops – Modeled) for Event 410

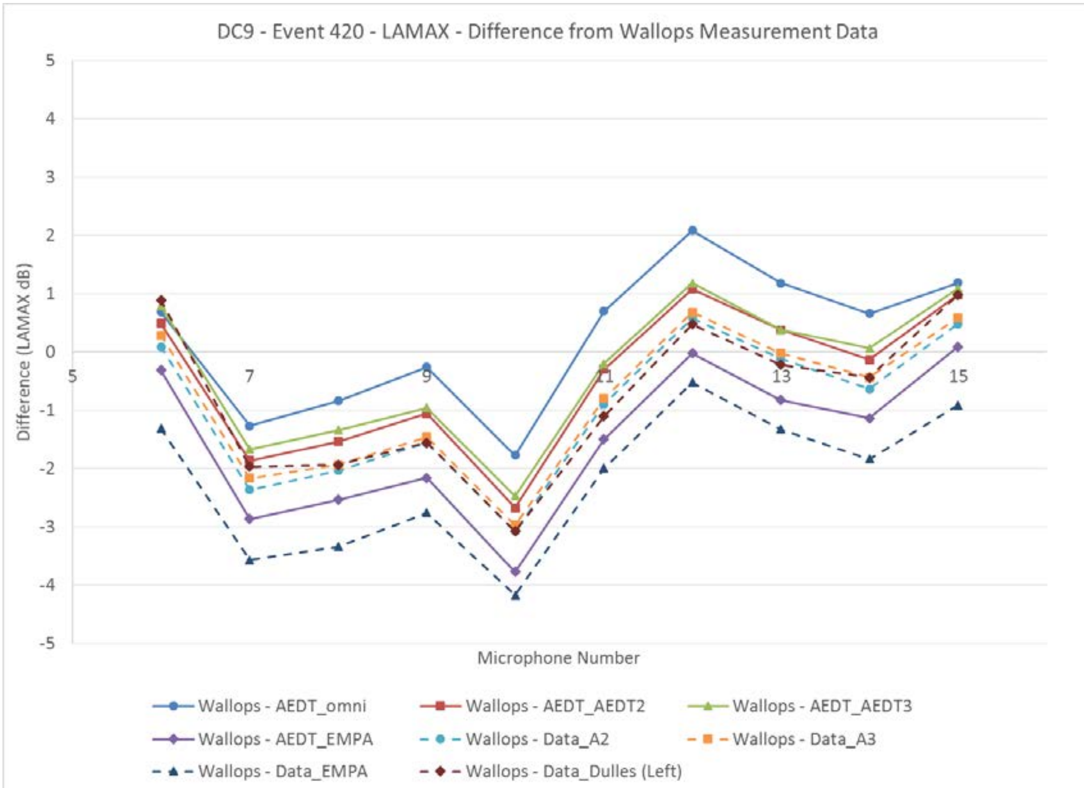

Figure 25. Phase 1 DC9-4 LAMAX Difference Results (Wallops – Modeled) for Event 420

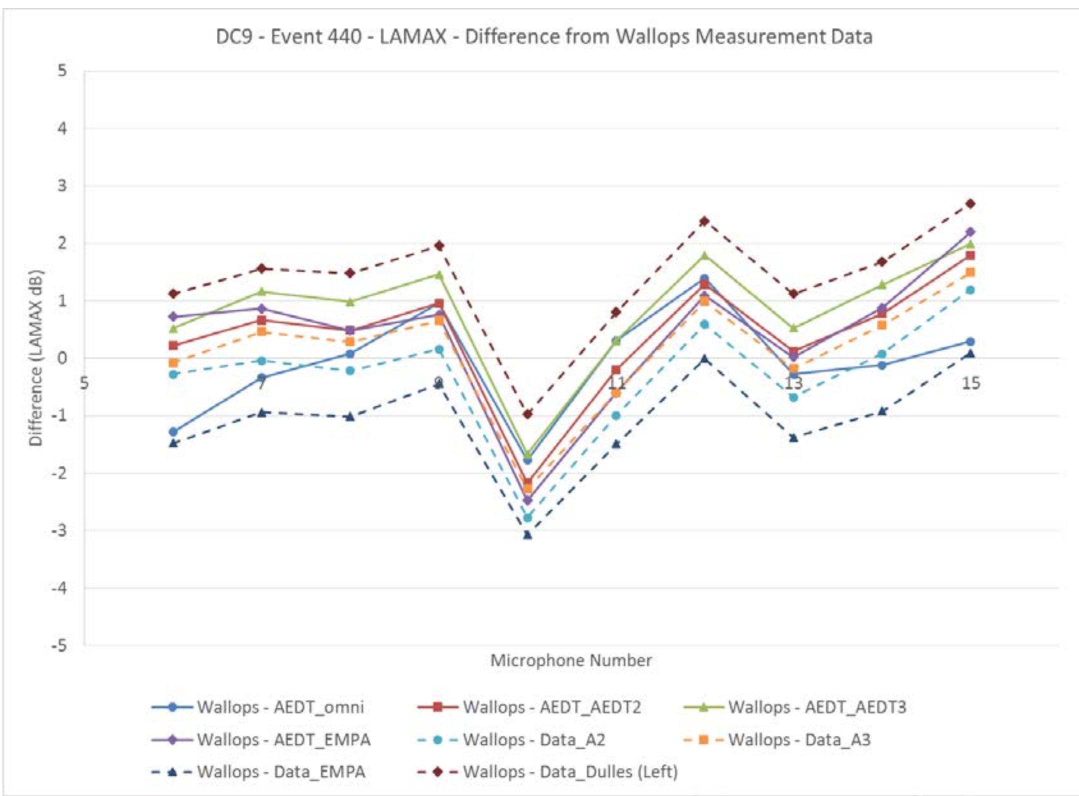

Figure 26. Phase 1 DC9-4 LAMAX Difference Results (Wallops – Modeled) for Event 440

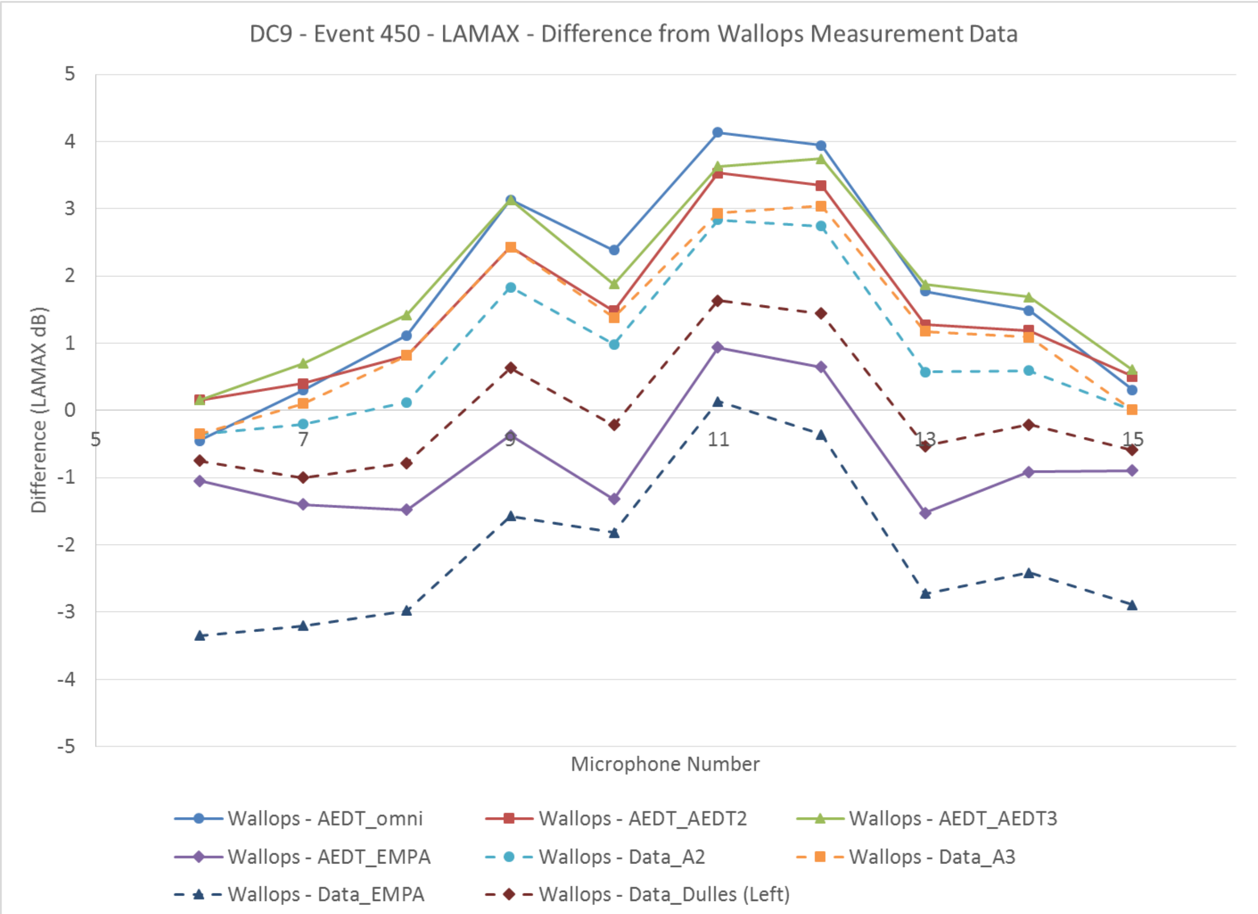

Figure 27. Phase 1 DC9-4 LAMAX Difference Results (Wallops – Modeled) for Event 450

9.3 Appendix: Phase 2 Results

This appendix includes the Phase 2 noise difference results for each event.

Table 296. Phase 2 DC9-4 SEL Difference Results (Wallops – Modeled) by Event for the Wallops 100 Series

			Diff SEL in dBA (Wallops Data - Measurement Results)				
Event	Aircraft	POI	AEDTSC_OMNI	AEDTSC-SOTR3	Data_SOTR3	Data_EMPA	Data_Dulles (Left)
110	DC93	P06	-0.46	-0.36	-0.26	-1.3	-0.36
110	DC93	P07	0.56	0.76	0.76	-0.28	0.66
110	DC93	P08	0.24	0.44	0.44	-0.5	0.34
110	DC93	P09	-1.14	-1.14	-1.04	-1.98	-1.14
110	DC93	P10	-0.44	-0.24	-0.24	-1.18	-0.34
110	DC93	P11	0	0	0	-0.84	0
110	DC93	P12	-0.93	-0.93	-0.83	-1.77	-0.93
110	DC93	P13	0.74	0.94	0.94	0	0.84
110	DC93	P14	0.37	0.57	0.57	-0.47	0.47
110	DC93	P15	0.39	0.49	0.59	-0.45	0.49
121	DC93	P06	-0.01	-0.01	-0.01	0.29	0.19
121	DC93	P07	0.57	0.57	0.57	0.67	0.67
121	DC93	P08	0.5	0.5	0.5	0.5	0.5
121	DC93	P09	-0.5	-0.6	-0.5	-0.5	-0.5
121	DC93	P10	-0.33	-0.23	-0.23	-0.13	-0.23
121	DC93	P11	0	0	0	0	0
121	DC93	P12	-0.38	-0.48	-0.38	-0.38	-0.38
121	DC93	P13	0.98	0.98	0.98	0.98	0.98
121	DC93	P14	0.94	0.94	0.94	1.04	1.04
121	DC93	P15	0.31	0.31	0.31	0.61	0.51
130	DC93	P06	0.4	0.4	0.3	0.3	0.2
130	DC93	P07	0.7	0.8	0.7	0.6	0.7
130	DC93	P08	0.38	0.48	0.38	0.38	0.38
130	DC93	P09	-0.76	-0.66	-0.76	-0.66	-0.66
130	DC93	P10	-0.3	-0.1	-0.1	-0.1	-0.2
130	DC93	P11	0	0	0	0	0
130	DC93	P12	-0.68	-0.58	-0.68	-0.58	-0.58
130	DC93	P13	0.74	0.84	0.74	0.74	0.74
130	DC93	P14	0.68	0.78	0.68	0.58	0.68
130	DC93	P15	-0.3	-0.3	-0.4	-0.4	-0.5

Table 26. Phase 2 DC9-4 SEL Difference Results (Wallops – Modeled) by Event for the Wallops 100 Series (cont.)

			Diff SEL in dBA (Wallops Data - Measurement Results)				
Event	Aircraft	POI	AEDTSC_OMNI	AEDTSC-SOTR3	Data_SOTR3	Data_EMPA	Data_Dulles (Left)
140	DC93	P06	0.78	1.28	1.18	2.28	1.48
140	DC93	P07	0.32	0.62	0.52	1.92	1.02
140	DC93	P08	0.31	0.51	0.41	1.41	0.71
140	DC93	P09	-0.27	-0.17	-0.17	0.43	0.03
140	DC93	P10	-0.26	-0.06	-0.06	0.24	-0.06
140	DC93	P11	0	0	0	0	0
140	DC93	P12	-0.26	-0.16	-0.16	0.44	0.04
140	DC93	P13	0.98	1.18	1.08	2.08	1.38
140	DC93	P14	0.44	0.74	0.64	2.04	1.14
140	DC93	P15	-0.06	0.44	0.34	1.44	0.64
150	DC93	P06	0.79	-0.01	-0.11	-0.01	-0.01
150	DC93	P07	0.65	-0.05	-0.05	-0.05	-0.25
150	DC93	P08	0.57	0.07	-0.03	-0.03	-0.23
150	DC93	P09	-0.25	-0.55	-0.65	-0.75	-0.85
150	DC93	P10	-0.17	-0.17	-0.27	-0.27	-0.47
150	DC93	P11	0	0	0	0	0
150	DC93	P12	-0.07	-0.37	-0.47	-0.57	-0.67
150	DC93	P13	0.86	0.36	0.26	0.26	0.06
150	DC93	P14	0.29	-0.41	-0.41	-0.41	-0.61
150	DC93	P15	0.09	-0.71	-0.81	-0.71	-0.71

Polar Source Analysis

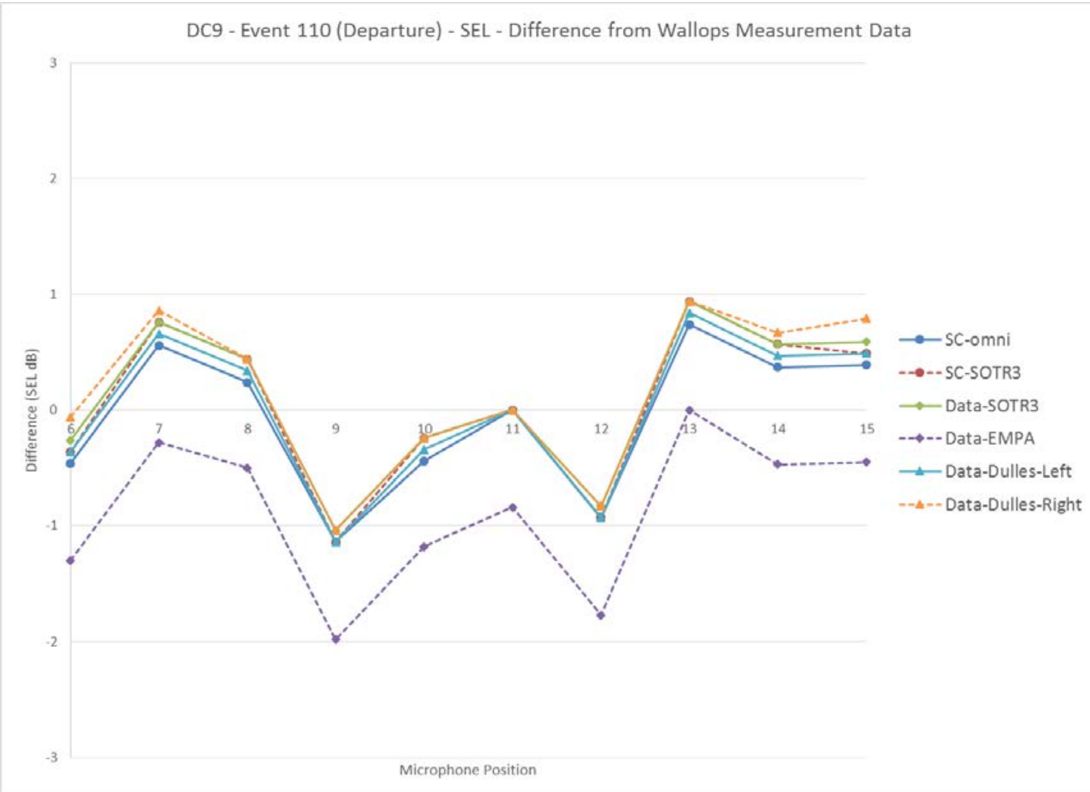

Figure 28. Phase 2 DC9-4 SEL Difference Results (Wallops – Modeled) for Event 110

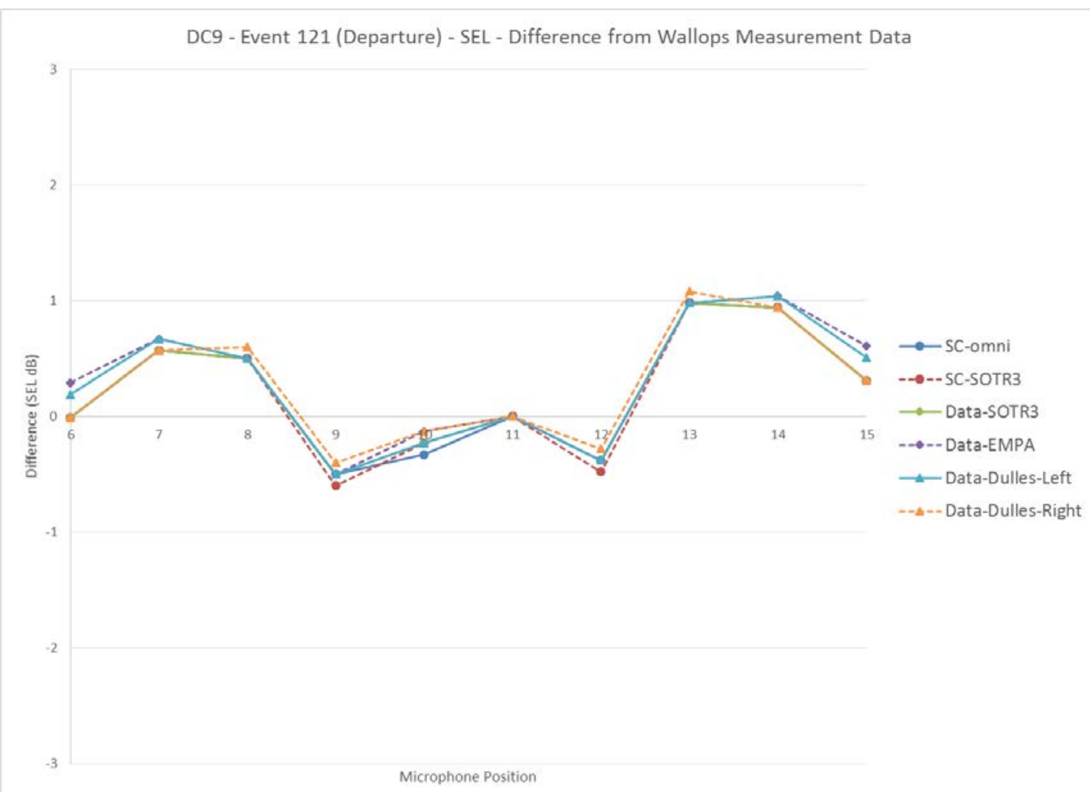

Figure 29. Phase 2 DC9-4 SEL Difference Results (Wallops – Modeled) for Event 121

Polar Source Analysis

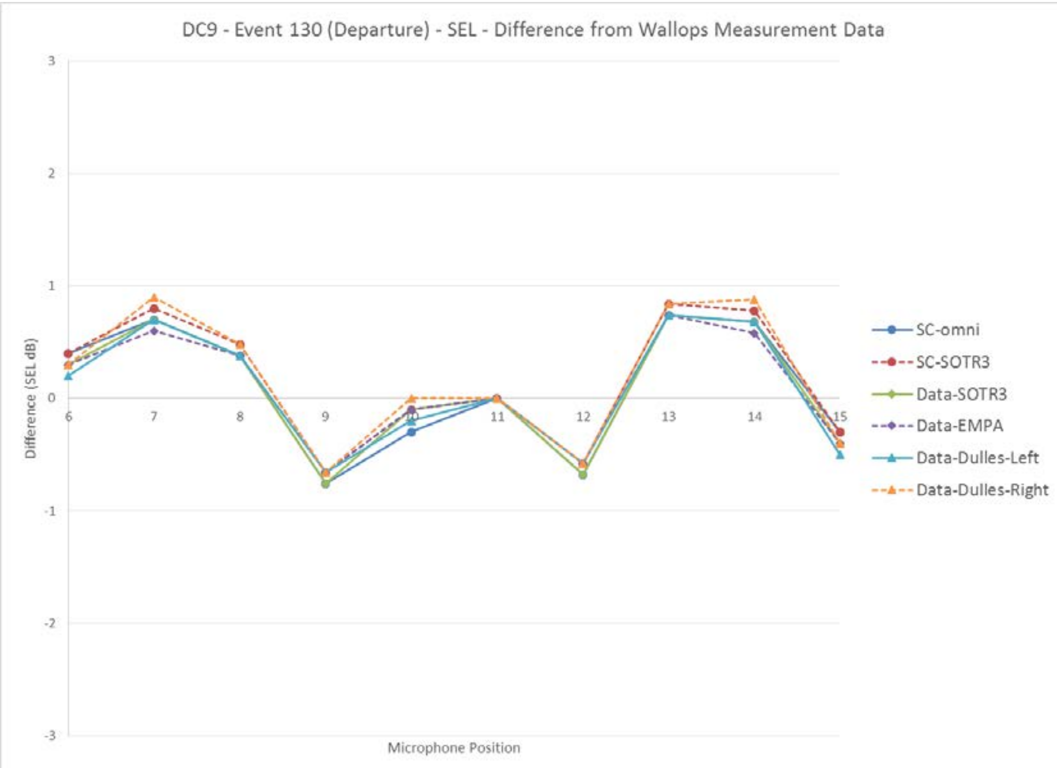

Figure 30. Phase 2 DC9-4 SEL Difference Results (Wallops – Modeled) for Event 130

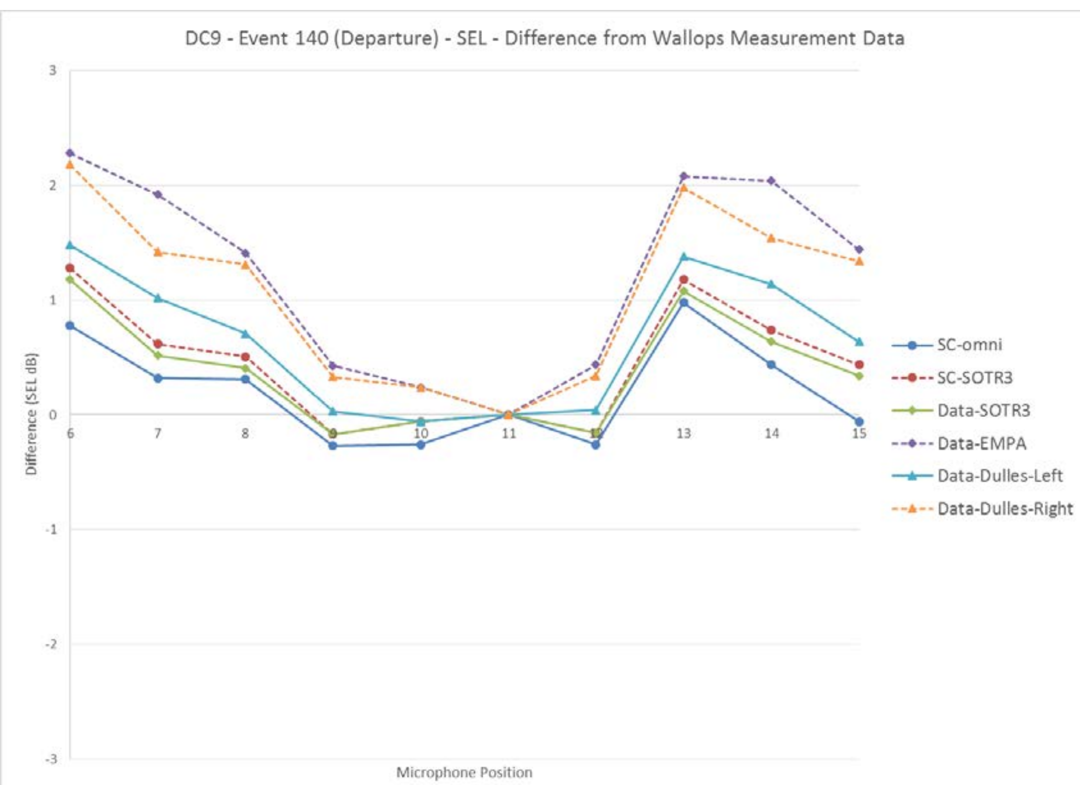

Figure 31. Phase 2 DC9-4 SEL Difference Results (Wallops – Modeled) for Event 140

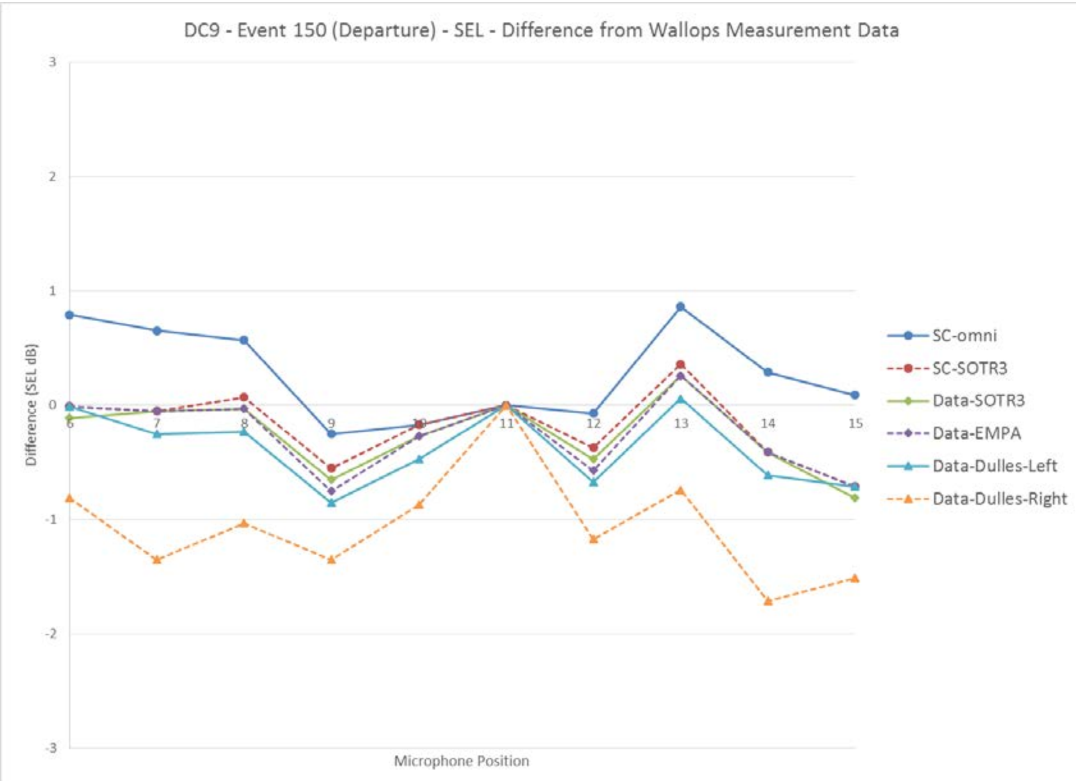

Figure 32. Phase 2 DC9-4 SEL Difference Results (Wallops – Modeled) for Event 150

Table 27. Phase 2 767-400 SEL Difference Results (Wallops – Modeled) by Event for the Wallops 100 Series

			Diff SEL in dBA (Wallops Data - Measurement Results)				
Event	**Aircraft**	**POI**	**AEDTSC_OMNI**	**AEDTSC-SOTR3**	**Data_SOTR3**	**Data_Dulles (Left)**	**Data_Dulles (Right)**
110	767-400	P06	-0.36	-0.36	-0.16	-0.16	-0.46
110	767-400	P07	0.05	0.05	0.15	0.25	-0.05
110	767-400	P08	0.09	0.09	0.19	0.29	-0.01
110	767-400	P09	-0.38	-0.48	-0.38	-0.28	-0.48
110	767-400	P10	-0.21	-0.11	-0.01	0.09	-0.01
110	767-400	P11	0	0	0	0	0
110	767-400	P12	-0.5	-0.5	-0.4	-0.3	-0.4
110	767-400	P13	0.82	0.82	0.92	0.92	0.82
110	767-400	P14	0.39	0.39	0.49	0.59	0.29
110	767-400	P15	-0.75	-0.75	-0.65	-0.55	-0.85

Table 27. Phase 2 767-400 SEL Difference Results (Wallops – Modeled) by Event for the Wallops 100 Series (cont.)

			Diff SEL in dBA (Wallops Data - Measurement Results)				
Event	Aircraft	POI	AEDTSC_OMNI	AEDTSC-SOTR3	Data_SOTR3	Data_Dulles (Left)	Data_Dulles (Right)
112	767-400	P06	0.06	-0.04	0.06	0.16	0.36
112	767-400	P07	0.86	0.76	0.86	0.86	0.96
112	767-400	P08	0.76	0.66	0.76	0.76	0.76
112	767-400	P09	-0.3	-0.3	-0.2	-0.3	-0.3
112	767-400	P10	-0.06	0.04	0.14	0.14	0.14
112	767-400	P11	0	0	0	0	0
112	767-400	P12	0.03	-0.07	0.03	0.03	-0.07
112	767-400	P13	0.88	0.78	0.88	0.88	0.98
112	767-400	P14	0.58	0.48	0.58	0.58	0.68
112	767-400	P15	-0.62	-0.62	-0.52	-0.52	-0.32
120	767-400	P06	-0.21	-0.11	-0.01	-0.21	-0.11
120	767-400	P07	0.17	0.17	0.27	0.07	0.17
120	767-400	P08	0.13	0.23	0.33	0.23	0.23
120	767-400	P09	-0.79	-0.79	-0.69	-0.79	-0.79
120	767-400	P10	-0.19	-0.09	0.11	0.01	0.01
120	767-400	P11	0	0	0	0	0
120	767-400	P12	-0.73	-0.73	-0.63	-0.73	-0.73
120	767-400	P13	0.54	0.54	0.64	0.54	0.54
120	767-400	P14	0.22	0.32	0.42	0.22	0.32
120	767-400	P15	-1.22	-1.12	-0.92	-1.22	-1.12
121	767-400	P06	0.02	0.02	0.12	0.22	-0.08
121	767-400	P07	0.34	0.34	0.34	0.44	0.24
121	767-400	P08	0.13	0.23	0.23	0.23	0.13
121	767-400	P09	-0.7	-0.6	-0.6	-0.6	-0.7
121	767-400	P10	-0.12	-0.02	0.08	0.08	-0.02
121	767-400	P11	0	0	0	0	0
121	767-400	P12	-0.69	-0.59	-0.59	-0.59	-0.69
121	767-400	P13	0.74	0.74	0.74	0.74	0.64
121	767-400	P14	0.54	0.64	0.54	0.64	0.44
121	767-400	P15	-0.81	-0.81	-0.71	-0.61	-0.91

Table 27. Phase 2 767-400 SEL Difference Results (Wallops – Modeled) by Event for the Wallops 100 Series (cont.)

Polar Source Analysis

			Diff SEL in dBA (Wallops Data - Measurement Results)				
Event	**Aircraft**	**POI**	**AEDTSC_OMNI**	**AEDTSC-SOTR3**	**Data_SOTR3**	**Data_Dulles (Left)**	**Data_Dulles (Right)**
140	767-400	P06	-0.22	0.38	0.48	0.08	0.88
140	767-400	P07	0.06	0.76	0.76	0.26	0.66
140	767-400	P08	-0.27	0.23	0.23	-0.17	0.13
140	767-400	P09	-1.1	-0.8	-0.8	-1	-0.9
140	767-400	P10	0.29	0.69	0.79	0.59	0.79
140	767-400	P11	0	0	0	0	0
140	767-400	P12	-0.36	-0.16	-0.06	-0.26	-0.16
140	767-400	P13	0.89	1.39	1.39	0.99	1.29
140	767-400	P14	-0.25	0.45	0.45	-0.05	0.45
140	767-400	P15	-1.08	-0.48	-0.38	-0.78	0.12
150	767-400	P06	-0.15	0.25	0.35	-1.05	-0.05
150	767-400	P07	0.25	0.35	0.35	-0.35	0.15
150	767-400	P08	-0.27	-0.27	-0.27	-0.47	-0.37
150	767-400	P09	-0.29	-0.29	-0.29	-0.29	-0.29
150	767-400	P10	0.79	0.99	0.99	0.99	0.99
150	767-400	P11	0	0	0	0	0
150	767-400	P12	-0.25	-0.25	-0.35	-0.45	-0.35
150	767-400	P13	0.62	0.72	0.72	0.22	0.62
150	767-400	P14	-0.22	-0.12	-0.02	-0.92	-0.22
150	767-400	P15	-1.08	-0.68	-0.48	-1.98	-0.88
160	767-400	P06	0.03	0.13	0.13	0.23	0.43
160	767-400	P07	0.02	0.02	0.02	0.12	0.12
160	767-400	P08	-0.02	0.08	0.08	0.08	0.08
160	767-400	P09	-0.79	-0.79	-0.69	-0.79	-0.69
160	767-400	P10	0	0.1	0.2	0.2	0.2
160	767-400	P11	0	0	0	0	0
160	767-400	P12	-0.2	-0.2	-0.2	-0.2	-0.3
160	767-400	P13	1.52	1.52	1.52	1.52	1.52
160	767-400	P14	0.34	0.34	0.44	0.34	0.34
160	767-400	P15	-0.69	-0.69	-0.69	-0.69	-0.59

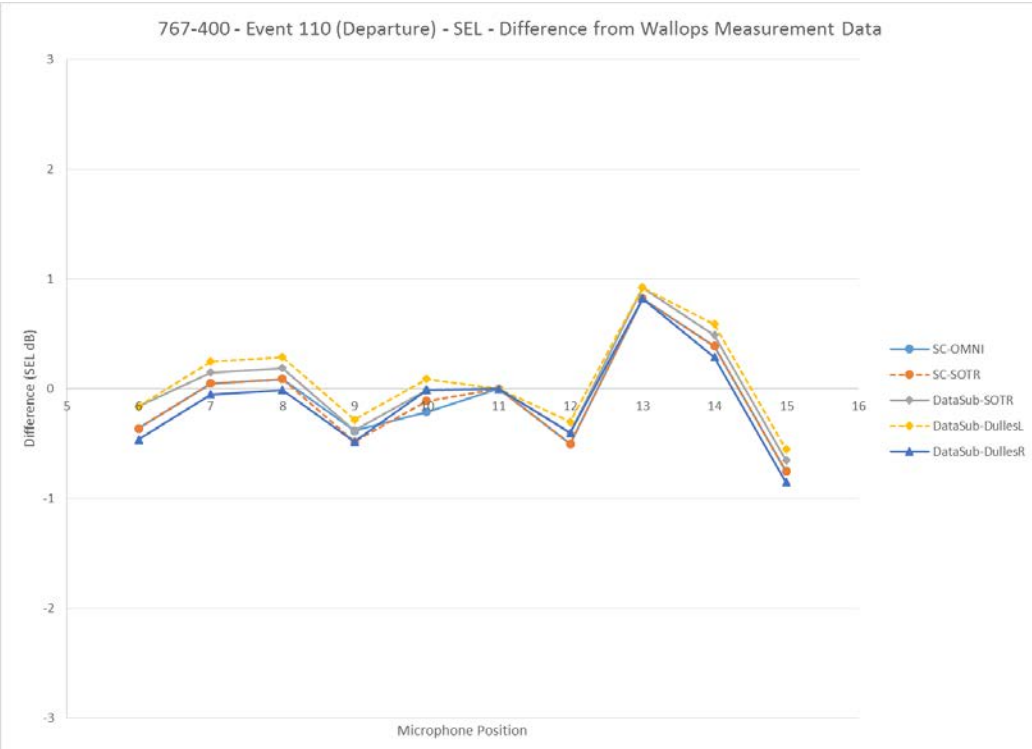

Figure 33. Phase 2 767-400 SEL Difference Results (Wallops – Modeled) for Event 110

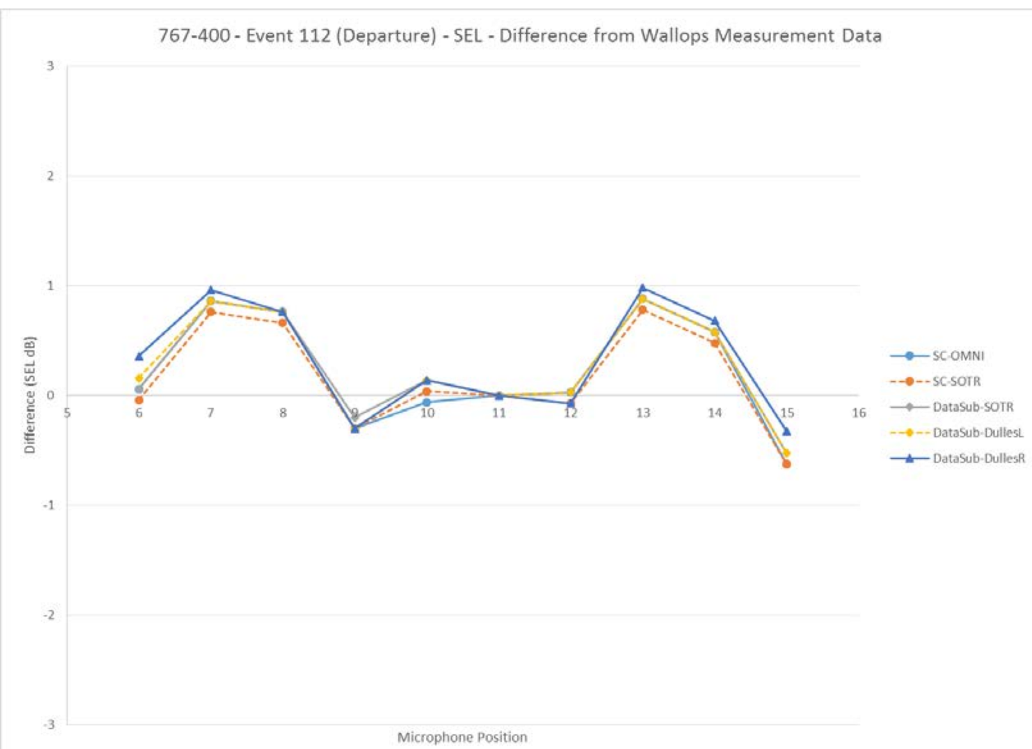

Figure 34. Phase 2 767-400 SEL Difference Results (Wallops – Modeled) for Event 112

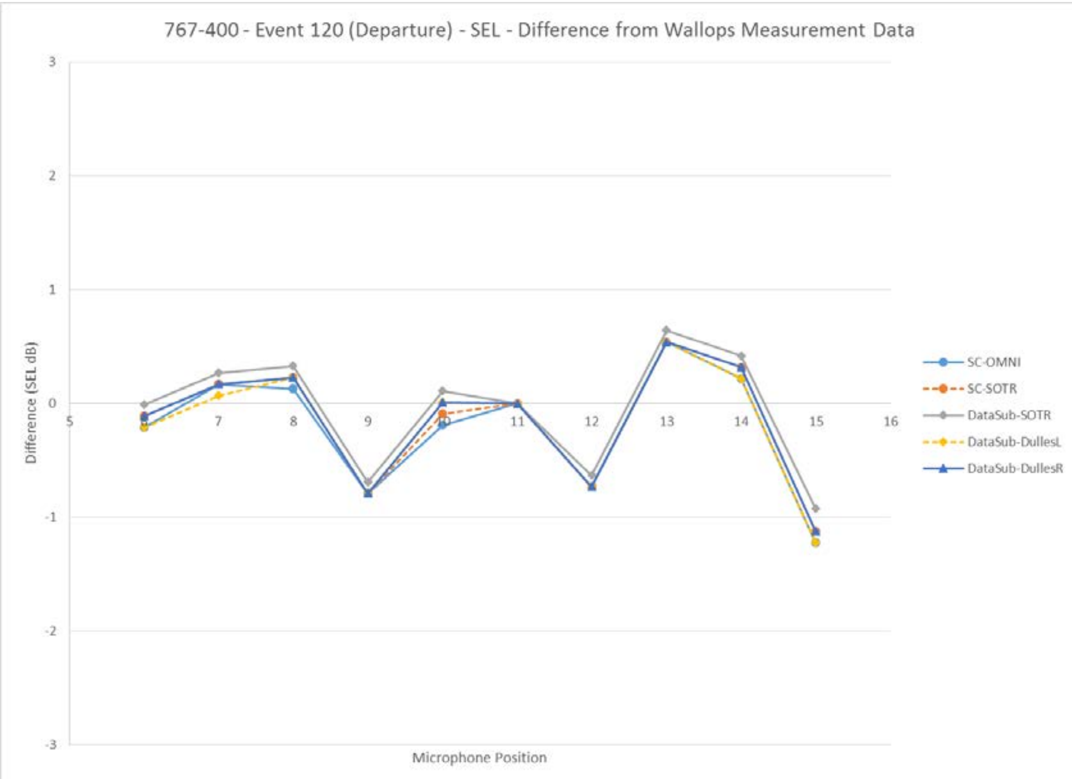

Figure 35. Phase 2 767-400 SEL Difference Results (Wallops – Modeled) for Event 120

Figure 36. Phase 2 767-400 SEL Difference Results (Wallops – Modeled) for Event 121

Polar Source Analysis

Figure 37. Phase 2 767-400 SEL Difference Results (Wallops – Modeled) for Event 140

Figure 38. Phase 2 767-400 SEL Difference Results (Wallops – Modeled) for Event 150

Polar Source Analysis

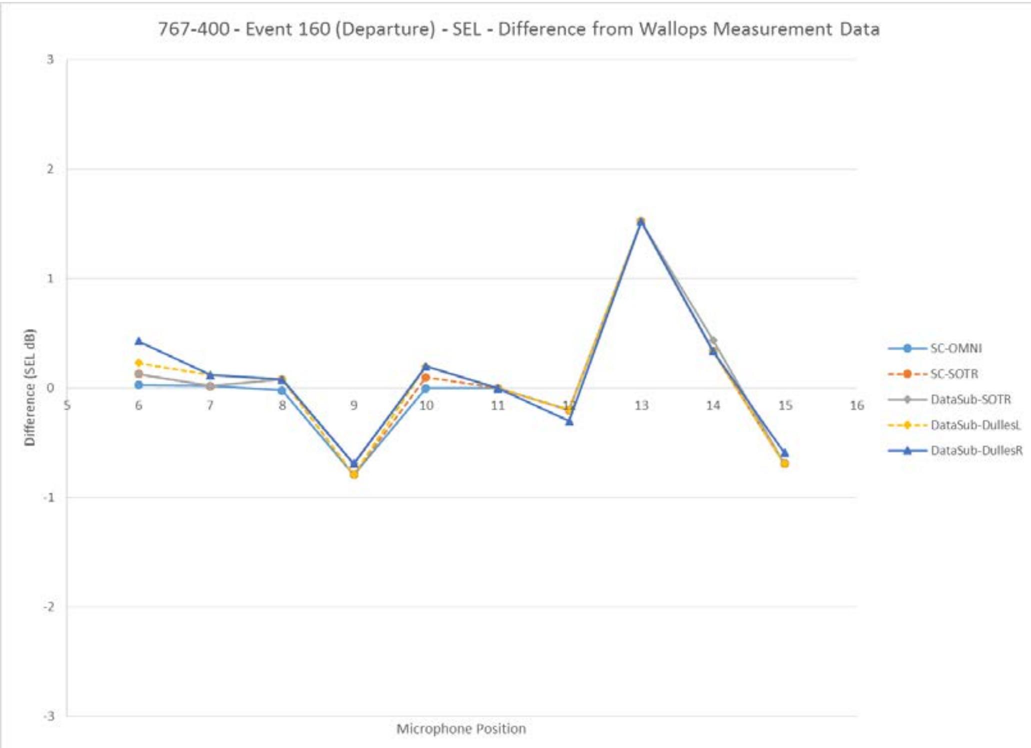

Figure 39. Phase 2 767-400 SEL Difference Results (Wallops – Modeled) for Event 160

Table 28. Phase 2 767-400 SEL Difference Results (Wallops – Modeled) by Event for the Wallops 300 Series

			Diff SEL in dBA (Wallops Data - Measurement Results)				
Event	**Aircraft**	**POI**	**AEDTSC_OMNI**	**AEDTSC-SOTR3**	**Data_SOTR3**	**Data_Dulles (Left)**	**Data_Dulles (Right)**
310	767-400	P06	0.37	0.77	0.77	0.27	0.47
310	767-400	P07	0.6	0.8	0.8	0.6	0.7
310	767-400	P08	0.77	0.87	0.87	0.77	0.77
310	767-400	P09	-0.19	-0.19	-0.19	-0.19	-0.19
310	767-400	P10	-0.64	-0.44	-0.44	-0.54	-0.44
310	767-400	P11	0	0	0	0	0
310	767-400	P12	-0.25	-0.15	-0.15	-0.25	-0.25
310	767-400	P13	1.62	1.72	1.72	1.62	1.72
310	767-400	P14	0.29	0.39	0.39	0.29	0.29
310	767-400	P15	0.13	0.43	0.43	0.03	0.13

Table 28. Phase 2 767-400 SEL Difference Results (Wallops – Modeled) by Event for the Wallops 300 Series (cont.)

			Diff SEL in dBA (Wallops Data - Measurement Results)				
Event	Aircraft	POI	AEDTSC_OMNI	AEDTSC-SOTR3	Data_SOTR3	Data_Dulles (Left)	Data_Dulles (Right)
321	767-400	P06	0.6	0.4	0.4	0.7	0.2
321	767-400	P07	0.93	0.73	0.73	0.93	0.63
321	767-400	P08	0.92	0.82	0.82	0.92	0.72
321	767-400	P09	0.24	0.14	0.14	0.14	0.04
321	767-400	P10	-0.19	-0.19	-0.19	-0.09	-0.19
321	767-400	P11	0	0	0	0	0
321	767-400	P12	-0.26	-0.26	-0.26	-0.26	-0.36
321	767-400	P13	1.3	1.2	1.2	1.3	1.1
321	767-400	P14	0.98	0.78	0.78	0.98	0.68
321	767-400	P15	-0.43	-0.63	-0.63	-0.33	-0.83
330	767-400	P06	-0.22	-0.32	-0.42	-0.12	-0.52
330	767-400	P07	-0.36	-0.36	-0.46	-0.26	-0.56
330	767-400	P08	0.26	0.16	0.16	0.26	0.16
330	767-400	P09	-1.22	-1.22	-1.32	-1.22	-1.32
330	767-400	P10	-0.61	-0.51	-0.61	-0.51	-0.61
330	767-400	P11	0	0	0	0	0
330	767-400	P12	-1.09	-1.09	-1.19	-1.09	-1.19
330	767-400	P13	0.72	0.62	0.52	0.72	0.52
330	767-400	P14	-0.13	-0.13	-0.23	-0.03	-0.33
330	767-400	P15	-1.52	-1.62	-1.82	-1.52	-1.92
340	767-400	P06	1.95	2.15	2.25	2.75	3.35
340	767-400	P07	1.52	1.92	2.02	2.12	2.72
340	767-400	P08	1.26	1.76	1.86	1.66	2.06
340	767-400	P09	-0.54	-0.14	-0.04	-0.34	-0.04
340	767-400	P10	0.21	0.71	0.71	0.51	0.71
340	767-400	P11	0	0	0	0	0
340	767-400	P12	0.11	0.31	0.31	0.21	0.31
340	767-400	P13	1.17	1.67	1.77	1.47	1.67
340	767-400	P14	1.11	1.51	1.61	1.51	2.01
340	767-400	P15	-1	-0.5	-0.5	-0.2	0.6

Table 28. Phase 2 767-400 SEL Difference Results (Wallops – Modeled) by Event for the Wallops 300 Series (cont.)

Polar Source Analysis

			Diff SEL in dBA (Wallops Data - Measurement Results)				
Event	Aircraft	POI	AEDTSC_OMNI	AEDTSC-SOTR3	Data_SOTR3	Data_Dulles (Left)	Data_Dulles (Right)
350	767-400	P06	1.05	1.85	1.75	0.75	1.55
350	767-400	P07	1.03	1.53	1.53	0.63	1.13
350	767-400	P08	0.42	0.72	0.62	0.12	0.42
350	767-400	P09	-0.35	-0.15	-0.15	-0.45	-0.35
350	767-400	P10	-0.5	-0.1	-0.2	-0.4	-0.3
350	767-400	P11	0	0	0	0	0
350	767-400	P12	-0.59	-0.39	-0.49	-0.69	-0.59
350	767-400	P13	0.73	1.03	1.03	0.53	0.73
350	767-400	P14	0.25	0.85	0.75	-0.05	0.45
350	767-400	P15	-0.76	-0.06	-0.06	-1.16	-0.36
360	767-400	P06	0.65	0.85	0.85	0.95	1.05
360	767-400	P07	1.35	1.55	1.55	1.45	1.55
360	767-400	P08	0.87	0.97	0.97	0.87	0.97
360	767-400	P09	-0.72	-0.62	-0.52	-0.72	-0.72
360	767-400	P10	-0.58	-0.38	-0.38	-0.48	-0.38
360	767-400	P11	0	0	0	0	0
360	767-400	P12	0.92	0.82	0.82	0.82	0.82
360	767-400	P13	2	2	2	2	2
360	767-400	P14	1.53	1.53	1.53	1.43	1.43
360	767-400	P15	0.1	0.2	0.2	0.1	0.1

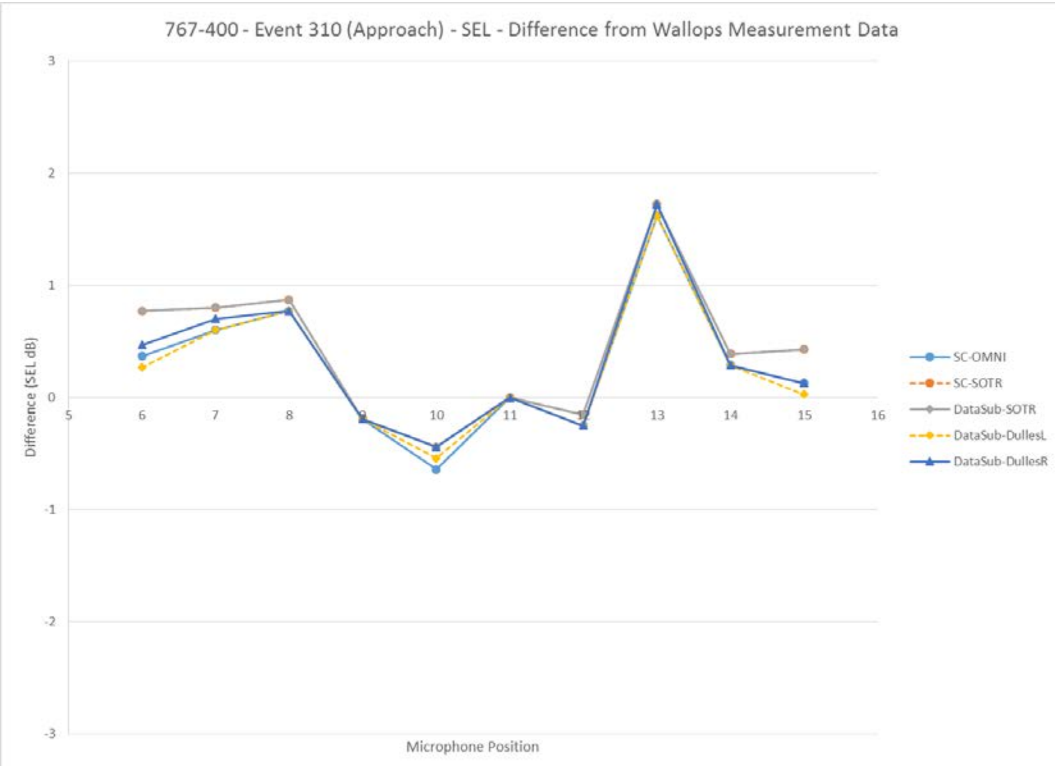

Figure 40. Phase 2 767-400 SEL Difference Results (Wallops – Modeled) for Event 310

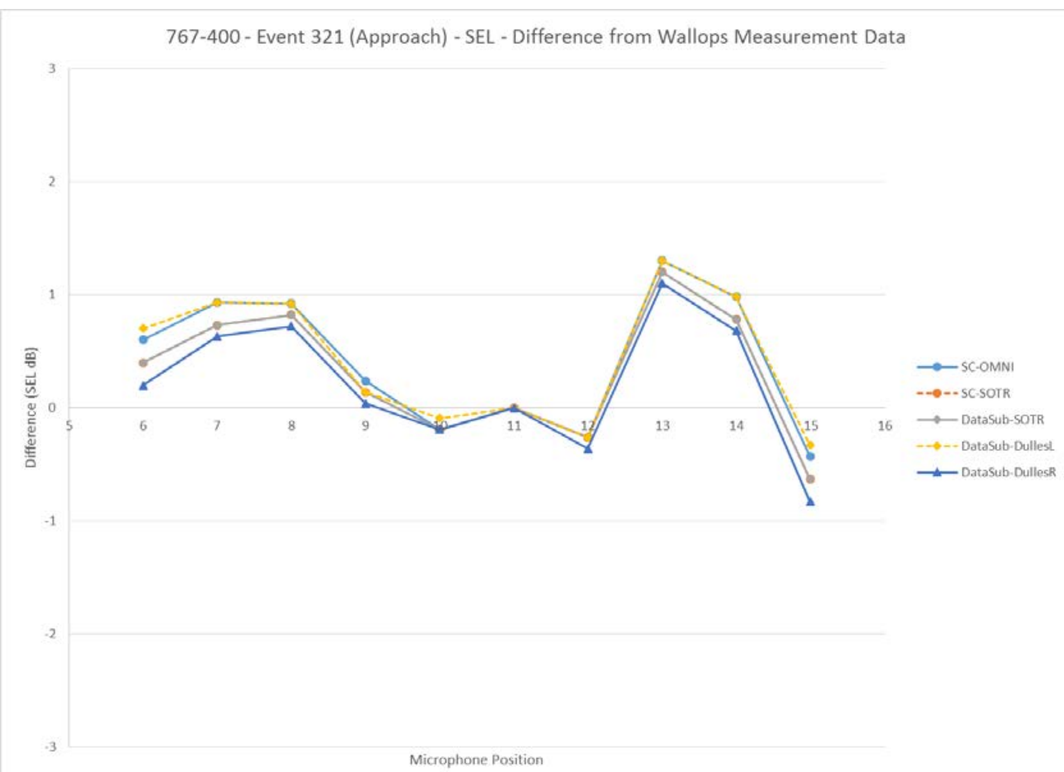

Figure 41. Phase 2 767-400 SEL Difference Results (Wallops – Modeled) for Event 321

Polar Source Analysis

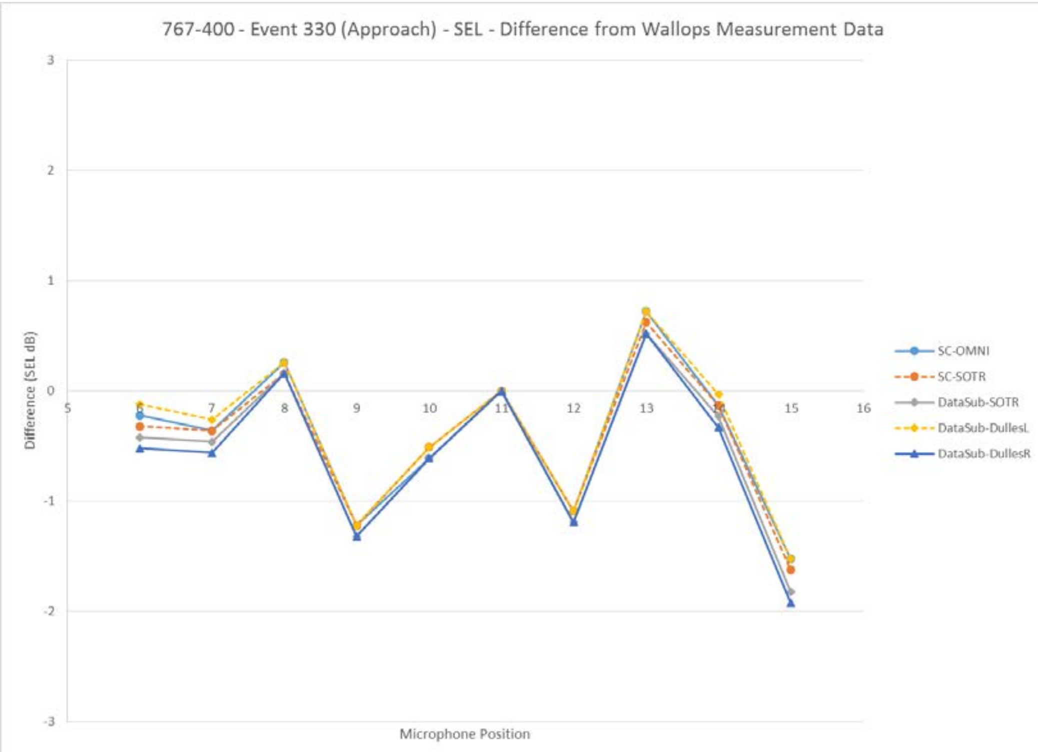

Figure 42. Phase 2 767-400 SEL Difference Results (Wallops – Modeled) for Event 330

Figure 43. Phase 2 767-400 SEL Difference Results (Wallops – Modeled) for Event 340

Polar Source Analysis

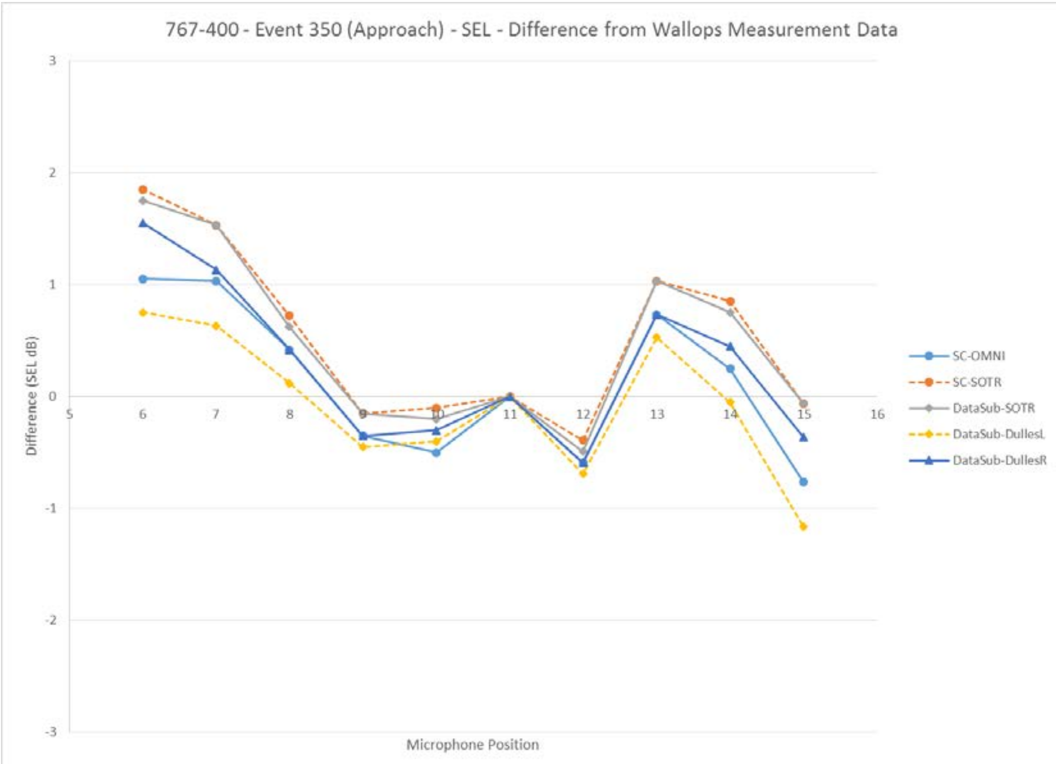

Figure 44. Phase 2 767-400 SEL Difference Results (Wallops – Modeled) for Event 350

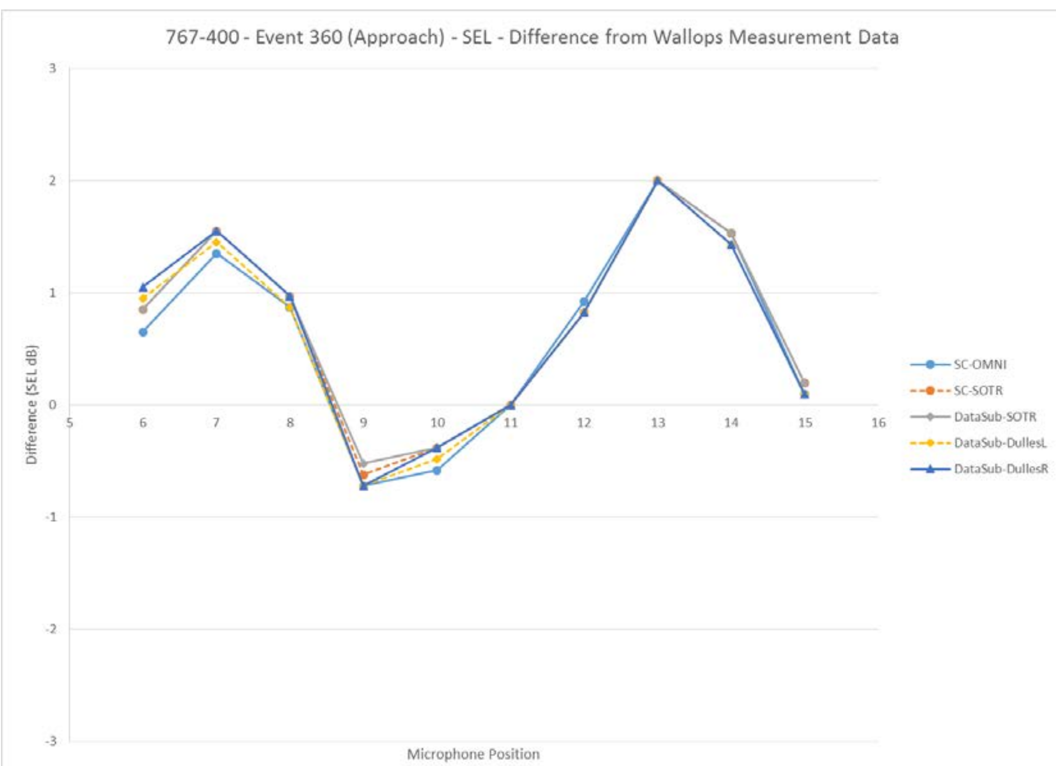

Figure 45. Phase 2 767-400 SEL Difference Results (Wallops – Modeled) for Event 360